Politecnico di Torino

Developing a hydrometallurgical process to integrate a Cathode Active Materials (CAM) synthesis step into the recycling process of spent Li-ion batteries containing nickel, cobalt, and manganese.

Master Thesis

Marlo Angelo Tito

Laurea Magistrale Ingegneria Energetica e Nucleare

Supervisors

Dr. Nestor Antuñano – CIC energiGUNE

Prof. Silvia Fiore, DIATI – Politecnico di Torino

UNIVERSITÉ DE LORRAINE

CIC energiGUNE

MEMBER OF BASQUE RESEARCH & TECHNOLOGY ALLIANCE

Acknowledgement

I would like to thank everyone who made this master's thesis internship possible. First to CIC energiGUNE for allowing me to work on this topic and especially to my industrial supervisor, Dr. Nestor Antuñano, for his guidance throughout stay in the research center. Thank you for making me feel welcome in the research group and making this a smooth and enjoyable experience. I would also like to thank the lab technician, Cristina Balza de Vallejo Díaz, for guiding me through the hands-on laboratory activities.

I am also sincerely grateful to Prof. Silvia Fiore, for accepting to be my academic supervisor. Her insights and comments have helped greatly progress this project. I appreciate the time she has taken to improve my study.

To the DENSYS consortium, Prof. Fabrice Lemoine, M. Heathcliff Demaie and Mme. Samira Menouar, and Prof. Marta Gandiglio, thank you for making this experience possible. This has been a great two years, and I could not thank you enough for having me on this program.

Lastly, I would like to thank the people who have been with me throughout the journey – my family, my friends, and my classmates from DENSYS. Thank you for your support in times of doubt and anxiety. Just know that you are my motivation as to why I strive to do well in my studies

This has been a wonderful learning experience, and I am looking forward to what comes next.

Table of Contents

List of Figures

List of Tables

List of Appendix Tables

Abstract

TITO, MARLO ANGELO MONES. Department of Energy "Galileo Ferraris", Politecnico di Torino. July 2024. **Developing a hydrometallurgical process to integrate a cathode active materials (cam) synthesis step into the recycling process of spent li-ion batteries containing nickel, cobalt, and manganese.**

Advisers: Dr. Nestor Antuñano, CIC energiGUNE

Prof. Silvia Fiore, Politecnico di Torino

The demand for lithium-ion batteries (LiB) is expected to exponentially increase in the coming years with the need to store energy to accommodate the energy transition movement. The most used raw materials for cathodic materials for LiBs are nickel, manganese, and cobalt. These metals, along with lithium, are now considered critical due to their exhausted usage and increasing economic importance. Recycling methods are established to alleviate the pressure on the demand for these materials. Hydrometallurgical methods recover the cathode active materials (CAM) in their precursor form, while lithium is recovered with low yield and purity. This study aims to integrate a lithium-recovery step in the hydrometallurgical recovery process of spent LiBs by increasing the yield and purity of lithium. This can be done using two ways: precipitation with sodium carbonate or with carbon dioxide gas to obtain lithium carbonate. Optimal reaction parameters were noted with respect to the yield and purity of the lithium carbonate. The recovered Li2CO3 was relithiated with the recycled CAM to synthesize a NMC battery. To validate the integration of this recovery step to the hydrometallurgical process, electrochemical testing was done to assess the performance of the recycled battery. Lastly, the energy and chemical costs were determined to evaluate the economic viability of the lithium recovery step.

Introduction

Problem Statement

The increasing urgency of the climate crisis has brought the attention of the need of energy transition to renewable energy sources (RES). One main drawback of renewable energy is the intermittent flow of energy. Typically, energy storage systems are in place to balance the supply of the RES and the typical power demand.

Electrochemical energy storage (i.e., batteries) is one of the principal ways of storing energy. One of the fastest growing groups of batteries are lithium-ion batteries (LiB). These batteries work based on electrochemical reactions of lithium-based compounds. While graphite is normally used as the anode, there exists a plethora of cathodic material alongside lithium. Examples of cathode material include oxides of cobalt, nickel-manganese-cobalt (NMC) and nickel-cobalt-aluminum (NCA).

The electrification of technologies has brought a substantial increase in demand for LiB. Figure 1 below shows the demand of LiBs in the US market from 2021 to 2030. The LiB demand in 2021 only accounts 7.6% of that of 2030, and most of the increase is attributed to the projection of electric vehicles (Gaines, 2023).

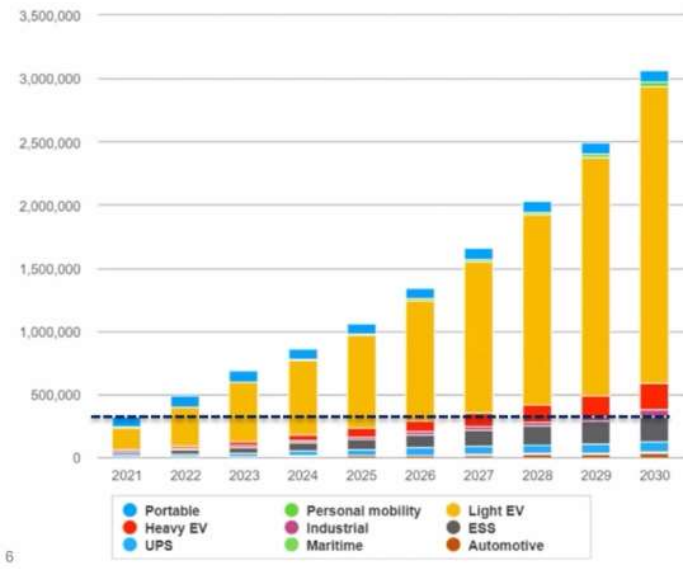

Figure 1. LiBs placed on the US market by application in tonnes (Gaines, 2023)

With the growing demand for LiB, pressure exists on the availability of the raw materials of these batteries. Lithium and the cathode active materials (nickel, manganese and cobalt) have been included in the 2020 list of EU Critical Raw Materials (CRMs). Materials in this list signify high economic and strategic importance, as well as a high supply risk in the EU economy. This alone is the core motivation of recycling batteries (Latini et al., 2022).

Currently, the EU has been dependent on imports from third countries where procurement may not be on par with ethical and environmental standards (Gaines, 2023).

From an environmental view, delayed disposal of spent batteries may result in them becoming hazardous waste. These batteries typically contain flammable organic solvents, polymeric layers, binders, metallic oxides and lithium ions (Latini et al., 2022). This may present a great challenge in waste management despite the high value of the raw materials.

Gaines et al. (2018) performed a life cycle analysis (LCA) on battery production and it was found that recycling reduces the energy use and overall emissions. Recovery of metals has been found to contribute the most to energy use reduction. Typically, fresh NMC materials are produced from low-concentration sulfide ores. This process is energy intensive and results in significant SO_x emissions.

The most common routes in recycling LiBs are the pyrometallurgical and hydrometallurgical methods, with the pyrometallurgical method being the most commercially available (Garole et al., 2020). In the hydrometallurgical route, recycled cathode active materials are recovered in their precursor forms as hydroxide salts, while lithium is discarded. Fresh lithium carbonate is used as there has not been any established method in recovering lithium efficiently. The initial concentration of lithium is too low to reach a high recovery rate using conventional precipitation methods (Zhao et al., 2019). This signifies that the flow of lithium in the battery production is still rather linear.

Objectives

This study aims to develop a lithium recovery step in the hydrometallurgical process of recycling lithium-ion batteries containing nickel, manganese and cobalt. On the other hand, the specific objectives are the following:

1. Conduct a parametric study on the factors (temperature, stoichiometry, precipitating agent) of lithium precipitation.
2. Develop a novelty process by using carbon dioxide as a precipitating agent.
3. Assess the recovered lithium with respect to its commercial value and the energy requirement of the process.
4. Integrate the recycled lithium into the relithiation step.
5. Characterize synthesized Li-NMC.

Scope

This study focuses on the hydrometallurgical route of recycling NMC-type of lithium-ion batteries. And the study only includes the recyclability of the cathodic material of the battery. Across the steps in the hydrometallurgical route, the steps considered start from the precipitation step of the cathode active materials until the synthesis of Li-NMC, wherein the lithium precipitation is emphasized.

Background

Lithium-Ion Batteries

Battery Chemistry

Lithium-ion batteries are a class of battery energy storage systems based on the redox reaction of lithium compounds. Like most electrochemical devices, it consists of the anode, cathode, electrolyte, separator and current collectors. Figure 2 shows the basic parts of LiB and the common materials used.

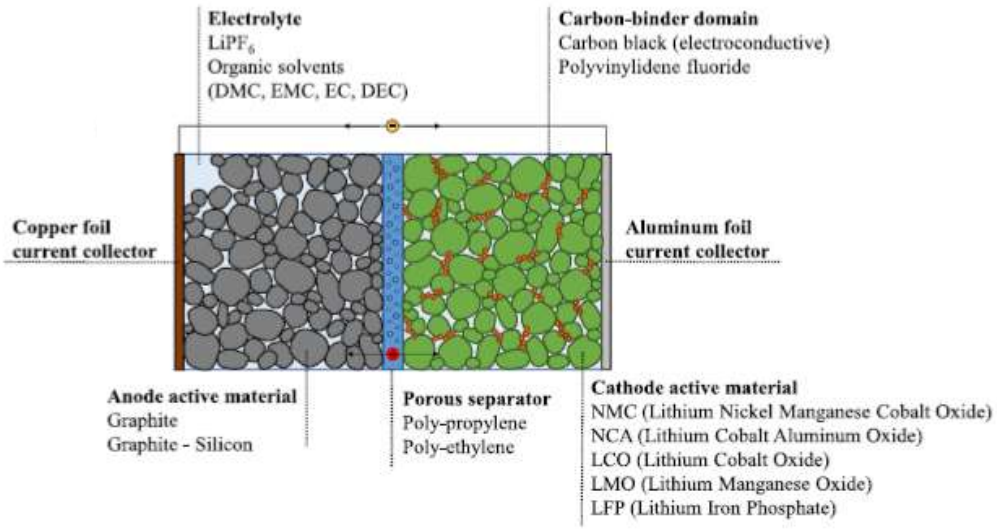

Figure 2. Parts of the LiB (Latini et al., 2022)

The electrolyte is composed of lithium hexafluorophosphate ($LiPF_6$) dissolved in an organic solvent such as ethylene carbonate or dimethyl carbonate. The polymer separator is placed to prevent contact between the anode and the cathode. The current collectors serve as the pathway for the electrons to travel between the electrodes, thereby consuming or generating current. Copper is used on the anode side while aluminum is used on the cathode side. The difference of the materials is due to the difference of redox potential of the anode and cathode.

The anode is typically made of graphite (a three-dimensional structure made of graphene layers). This is the positively charged component of the battery where oxidation occurs during the discharge phase and reduction occurs in the charging phase. In general, both natural and synthetic graphite are used on a commercial scale. Synthetic graphite is produced via baking of petroleum coke at 2500°C for several days. This results to a high purity (99% carbon), low thermal expansion and better thermal stability compared to natural graphite (Asenbauer et al., 2020).

Due to its higher purity and quality, synthetic graphite is used in EV applications while natural graphite is used in portable applications as these applications do not require a long product lifetime. Natural graphite is classified as a critical raw material which puts pressure on the production of synthetic graphite as the demand for LiB is significantly increasing (Asenbauer et al., 2020). Despite receiving less attention as recycling cathode and electrolyte materials, graphite recovery from spent LiB has been demonstrated with similar properties as that of pristine graphite(Sabisch et al., 2018).

Meanwhile, the cathode is the negatively charged component where the reduction reaction takes place during the discharge phase and the oxidation reaction at the charging phase. The cathodic materials are more diverse, such that LiBs are classified based on the cathode (Latini et al., 2022). Major cathode chemistries include oxides of Lithium Nickel-Manganese-Cobalt (NMC), Lithium Nickel-Cobalt-Aluminum (NCA), Lithium Cobalt (LCO), Lithium Manganese (LMO) and Lithium Iron Phosphate (LFP). Table 1 shows the electrochemical characteristics across the different cathode chemistries.

Table 1. LiB Cathode Chemistry (Or et al., 2020)

Cathode Material	**LCO**	**NMC**	**LMO**	**NCA**	**LFP**
Average potential (V vs. Li^0)	3.6	3.7	4.0	3.7	3.3
Gravimetric capacity (mAh/g at 0.1C)	145	170	120	200	165
Specific energy (Wh/cm^3)	550	600	496	700	589

The NMC cathode configuration is the most commonly chemistry used in EV applications. The cathode is represented as a compound of $LiNi_xMn_yCo_zO_2$, where x + y + z = 1. In recent years, NMC has become more economically and environmentally desirable as NMC batteries with less cobalt content are being developed. This decreases the cost of the battery, in addition to the decrease of environmental and ethical impacts (Davis & Demopoulos, 2023).

The proportions of the cathode active materials vary in NMC lithium batteries. This is used as the basis of naming NMC LiB. For example, NMC 111 refers to the 1:1:1 ratio of nickel, manganese and cobalt in the cathode. In this configuration, nickel, manganese and cobalt have an ideal oxidation state of +2, +3 and +4, respectively. Table 2 below shows the composition of NMC components with respect to its name and/or classification.

Table 2. NMC batteries composition (%wt/kWh) (Davis & Demopoulos, 2023)

Material	**NMC 111**	**NMC 532**	**NMC 622**	**NMC 811**
Lithium	0.141	0.136	0.118	0.1
Nickel	0.351	0.508	0.531	0.6
Cobalt	0.352	0.204	0.178	0.75
Manganese	0.328	0.285	0.166	0.07

Depending on the application, batteries are typically arranged into modules and packs to supply the energy and power demand. One NMC cell typically only has a voltage of 3.7 V as listed in Table 1. Cells are arranged into modules, and then modules are arranged into packs. There are three major configurations – cylindrical, prismatic and pouch. Figure 3 below shows examples of the different battery geometries.

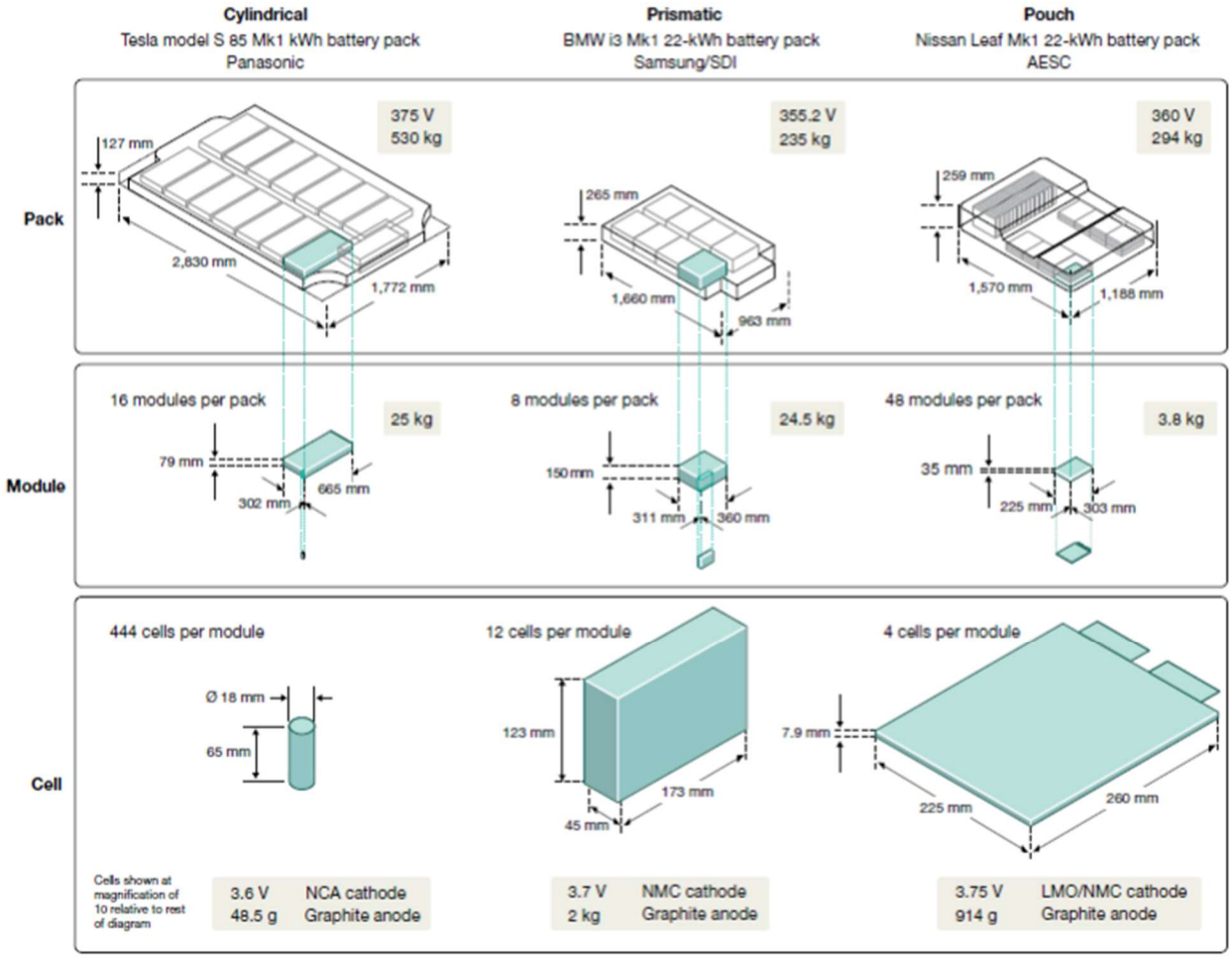

Figure 3. Cell geometries and battery packing (Harper et al., 2019)

These cell geometries have different advantages and disadvantages, which make them useful in different applications based on the desired qualities. For example, prismatic cells have a higher packing factor, but the thermal regulation is lacking (need for cooling equipment). Cylindrical cells have good scalability but need more maintenance. Lastly, pouch cells are easier to attached but there are issues with the cell's tendency to swell (Harper et al., 2019).

Battery geometries also affect the electrical connections of cells and modules into modules and packs, respectively. This relays to the energy requirement and difficulty of techniques into assembling battery systems. In addition, the thermal management of large battery systems depends on the arrangement of the battery packs.

The different arrangements of the battery pack and modules present different recycling challenges, particularly to the disassembly. For example, cylindrical and pouch cells are bonded into modules with epoxy resin, which is difficult to remove or recycle. Prismatic cells require special tools to remove its contents, as they require can opening and are more pressurized relative to cylindrical or pouch cells. Meanwhile, pouch cells are generally less problematic to open and easier to mechanically separate (Harper et al., 2019).

Criticality of LiB Raw Materials

In 2020, the European Commission presented a list of critical materials. This refers to the list of materials with a high supply risk while maintaining an economic and strategic importance of the region. The list includes and maintains magnesium and cobalt from 2017, with lithium being a new addition. Nickel is also being closely monitored due to its growing demand for battery raw materials (European Commission, 2020). The criticality of materials differs across regions as lithium is not considered to be critical in North America, for example, due to high supply.

Along with the critical raw material (CRM) list, the commission has also presented an action plan on CRM and a foresight study on CRM for strategic technologies and sectors in 2030 and 2050 outlooks. The action plan looks at the current and future challenges, along with the suggested actions to alleviate Europe's dependency from third countries through the diversification of the supply from all sources and improvement of resource efficiency and circularity while promoting responsible sourcing globally. Europe's high dependence on third countries places great risk and vulnerability of economic growth and security (Di Persio et al., 2022).. An extreme case is the region's dependence on rare earth minerals, of which around 98% is supplied through import.

This is the main driver of the need to recycle LiB - that is, to secure the EU's internal supply of metals and to lessen the dependence on import from other countries (Latini et al., 2022). Other than the question of demand, the analysis of CRMs also considers geopolitical factors that affect the future supply such as the geographical concentration or access to known CRM. China, for example, supplies 98-99% of rare earth minerals (Di Persio et al., 2022) to the European Union.

Figure 4 below shows the countries which supply CRMs to the EU. In the case of cobalt, the Democratic Republic of Congo (DRC) holds 60% of the world's cobalt resource. The cobalt mines in the country are dominated by Chinese-owned companies which gives these

companies security for cobalt supply over international companies. In addition, there have been severe human rights issues reported in the DRC including child labor, fatal accidents, and high corruption in cobalt mines (Gaines, 2023). Chile is the largest supplier of lithium with 78% of the supply share (European Commission, 2020).

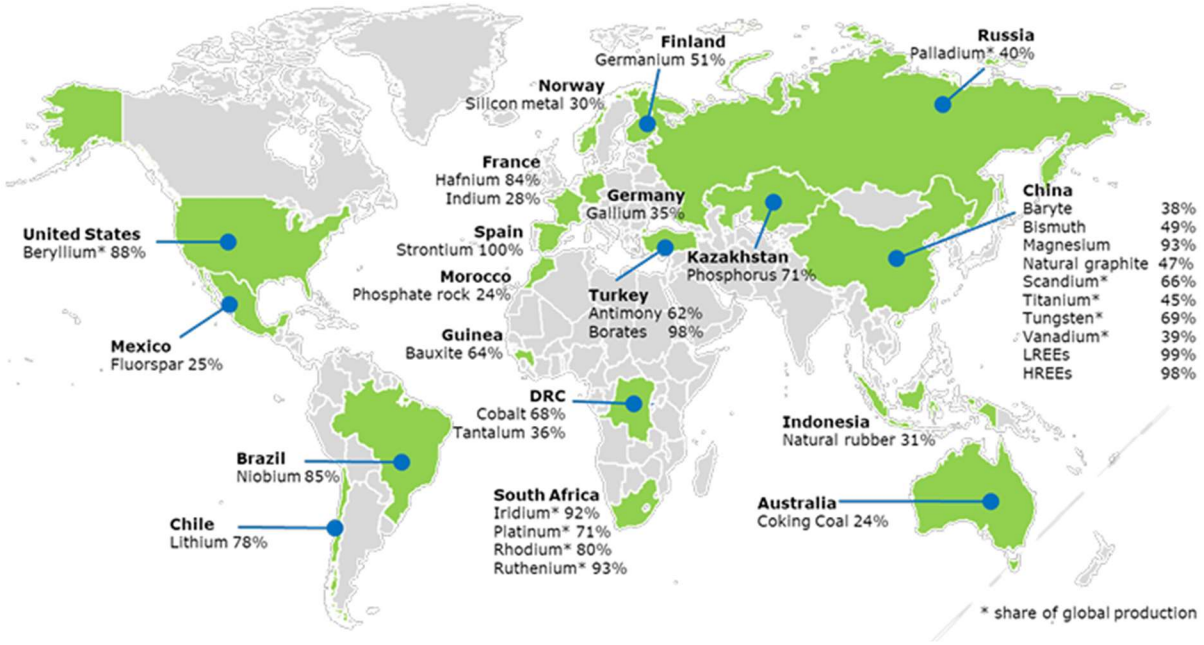

Figure 4. Largest Supplier Countries of CRMs to the EU (European Commission, 2020)

These CRMs are crucial to Europe's goal of energy transition through the shift to renewable energy and green technology. The progress of energy transition depends on the development of technologies, new infrastructure, automation, and artificial intelligence. And the EU depends on the application of CRMs to a significant degree for rollout of renewable energy to be possible. This makes the energy transition movement susceptible to disruptions in the supply (Di Persio et al., 2022). Electric vehicles are one of the fastest-growing technologies worldwide and it is facing higher risk of interruption due to the criticality of the materials used such as rare earth minerals, platinum, lithium and natural graphite.

One of the measures outlined in the commission's action plan is to exploit domestic reserves. But this obviously does not suffice the growing demand of CRMs considering the technological developments. Recycling is another important measure to mitigate the material supply risk. However, the industry for recycling lithium-ion batteries is only at its initiation stage and the ones that are of the largest scale, use energy-intensive processes to recycle batteries from electric vehicles (Di Persio et al., 2022).

Recycling Lithium-ion batteries

Table 3 below shows the typical battery composition of LiB, along with the main material used for each component. In addition to the criticality of the cathode-active materials, they also make up 65-70% of the cost of the battery despite making around a fourth of the battery's mass. The anode material is mostly dominated by graphite, making up 8-9% of the cost (Thompson et al., 2020).

Table 3. Components and Materials of LiB (Thompson et al., 2020; Velázquez-Martínez et al., 2019)

Battery Component	%w/w	Most Used Material	Cost, %
Case	~25%	Steel/plastics	4
Cathode	~27%	LiCoO2, LiNixMnyCozO2, LiMn2O4, LiNiO2, LiFePO4	65-70
Anode	~17%	Graphite/Li4Ti5O12	8-9
Copper and aluminium foils and current collectors	~13%	Cu/Al	3
Electrolyte	~10%	Solution of LiPF6, LiBF4, LiClO4, and LiSO2 dissolved in propylene carbonate, ethylene carbonate, or dimethyl sulfoxide	1
Separator	~4%	Microporous polypropylene	4
Binder	~4%	Polivinylidene Difluoride (PVDF)	8-9

Different methods already exist with regards to battery recycling – namely these are the pyrometallurgical process, hydrometallurgical process and direct recycling. These recycling routes consist of a series of unit operations starting from the EoL phase of batteries. Typically, the cathode active materials are the main components that are recycled for their high-value and limited supply, although recycling anodic materials have also proven to be feasible and cost-effective (Sabisch et al., 2018; Zhang et al., 2019).

Pretreatment process

As outlined by Latini et al. (2022), the pretreatment process of recycling batteries consists of physical and chemical treatments where the metallic casing and plastic components are separated from the battery. First, a deactivation step is applied to reduce risks of flammability, short-circuiting and electroshock. The latter is a higher risk of EV due to the magnitude of working voltage. This is done by over-discharging the battery in a conductive liquid (usually NaCl brine) or through an electrical device to recover 20% of the remaining energy that is given to the grid or to provide heat for the plant. Then, the electrolyte material is deactivated by thermal volatilization or freezing.

Then, the spent batteries undergo pretreatment processes such as size reduction of the battery and electrolyte separation. For large battery systems, the battery is manually

disassembled to recover system components such as housing, cables, and battery management unit. Typically, battery geometries differ too much for automation to be possible at this step (Thompson et al., 2020).

The crushing step of the battery modules is done under vacuum, or N_2/CO_2 atmosphere with a shredder consisting of a single rotary shear with forced feeding, at a set particle size of 20 mm (Or et al., 2020). The crushing step generates exhaust gases composed of volatile organic compounds (VOCs) and toxic HF gas from the binder and lithium salt decomposition. The remaining electrolyte. In either case, a post-combustion process is required due to the generation of HF gas from the decomposition of the conducting $LiFP_6$ salt in the electrolyte (Latini et al., 2022)., which remains a flammable hazard, can be removed through extraction or thermal drying. Grützke et al., 2015 were able to perform an alternative extraction method using sub-critical CO_2 at 60 bar and 25°C, with thermal drying being operated in 80-140°C at 100-300 mbar.

Then mechanical separation is performed to separate the plastic and foil fractions from the battery parts through a combination of multi-step mechanical separations such as air-sifting, crushing, and sieving. The battery undergoes air classification where it separates heavy and light fractions. The heavy fraction consists of mostly housing and module materials while the light fraction consists of anodic and cathodic materials, along with the plastic separators. The heavy fraction is subjected to magnetic separation to recover the steel and aluminum casing.

The light fraction then undergoes further size reduction and sieving to separate the electrode active materials. The powder that results from this process is called the black mass, consisting of electrode coatings (97% wt.), copper (1.9%), aluminum (0.8%) and steel (0.3%). This powder serves as the starting point for the recycling of most battery recycling routes such as the hydrometallurgical route and direct recycling.

Pyrometallurgical Method

The pyrometallurgical method of recycling LiB is based on the smelting process of the whole battery at high temperatures (at T = 1500°C) to recover an alloy of metals, and then a hydrometallurgical refinery follows to recover the CAMs. Throughout the smelting process, the electrolyte and plastic/graphite material are removed at low and high temperatures, respectively. Meanwhile, the slag consists of the lithium, CAM and the casing materials in which the lithium ends up in the low-value slag with the current collectors (Latini et al., 2022).

This low-value slag consisting of lithium, copper and aluminum is often used as additive materials in construction. Unlike other methods, this recycling pathway does not need an electrolyte deactivation step in the pretreatment stage as the electrolyte is vaporized from

the smelting process. It is also flexible in terms of battery geometry and type, even accepting batteries like Ni-metal hydride or primary Li (Latini et al., 2022).

Among all the processes, the pyrometallurgical method is the most established technologically and is available on an industrial scale. However, it is problematic for several reasons. First, carbon-based components such as the anode active material (graphite) and electrolyte are necessarily burnt. The recycled products also have low purity and CRMs recycled are downcycled, lowering its value. Moreover, the process itself is energy intensive, causing a net increase in greenhouse gas emissions (GHG) for all LiB chemistries throughout their life cycle (Latini et al., 2022).

Direct Recycling

Direct recycling approaches refer to the emerging processes that regenerate the cathode and anode materials without decomposing the battery into its constituents through acid leaching or high-temperature treatments. This method restores the lithium inventory in the CAM by preserving the particle morphology and crystalline structure. As such, the recycled products can be directly used in battery manufacturing (Latini et al., 2022).

One of the main challenges associated with direct recycling is the isolation of the electrode. Organic solvents such as N-Methyl-2-pyrrolidone can be used to extract the electrodes but purification and toxicity issues are persistent. An alternative process for this is through thermal decomposition of the binder but this produces HF which can damage the cathode and be hazardous to humans (Sloop et al., 2020).

In addition, methods are still being established on how to directly regenerate cathode active materials. Among LiB types, methods such as chemical and electrochemical lithiation have been performed on LFP batteries (Latini et al., 2022). One of the main challenges is to achieve the same mechanical and electrochemical performance. This might be a tradeoff with the cost due to the presence of impurities.

Hydrometallurgical Method

The hydrometallurgical route takes advantage of the differences in the solubilities of the metallic components in the battery. It uses a combination of acid leaching, solvent extraction and selective precipitation to recover metals from the spent batteries. The end products are high-purity metal salts which can be used as a precursor material to battery manufacturing (X. Chen et al., 2015).

Like the direct recycling method, this route also starts off with the pretreatment process to produce the black mass. The black mass then undergoes a series of hydrometallurgical unit operations and processes such as acid leaching, coprecipitation and neutralization. The

final product is the ionic salt precursors of NMC (i.e., hydroxides of cathode active materials). Latini et al. (2022) outlines the process of hydrometallurgical pathway of spent Li-NMC batteries below in Figure 5.

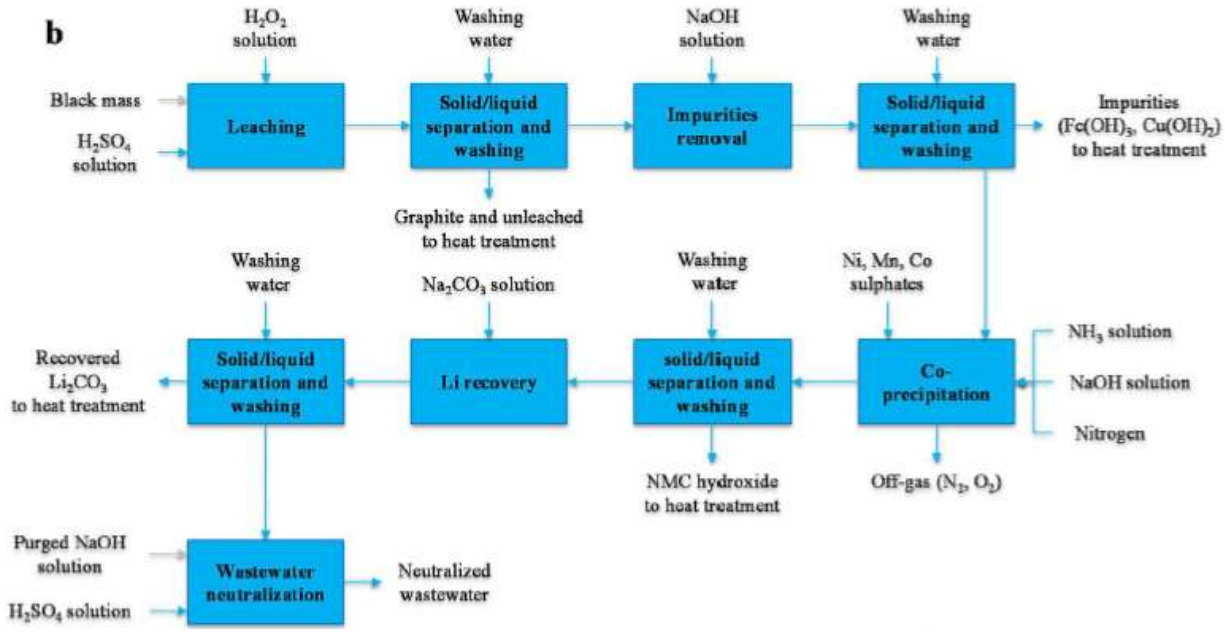

Figure 5. Hydrometallurgical method of recycling Li-NMC (Latini et al., 2022)

This process requires less energy as the working temperature is much lower than that of the pyrometallurgical method. The energy input is involved in the precipitation process, where the operating temperature does not exceed the boiling point of the water. In addition, due to the nature of the process, the crystalline cathode structure is disrupted even though the chemical identity of the CAM from the spent LiB is preserved (Latini et al., 2022).

Methodology

Hydrometallurgical method of recycling

Figure 6 shows the general schematic diagram of the hydrometallurgical process of recycling spent LiB-NMC. Starting with the black mass, the powder is dissolved with strong inorganic acids such as H_2SO_4 with added H_2O_2 to separate out the metallic ions (Mn^{2+}, Co^{3+}, Ni^{2+}, Li^{+} and other metallic impurities) from graphite. The addition of the strong acid maintains the mixture at an acidic pH. Hydrochloric acid can also be used in place of sulfuric acid but H_2SO_4 is more cost-effective (Jara & Kim, 2020).

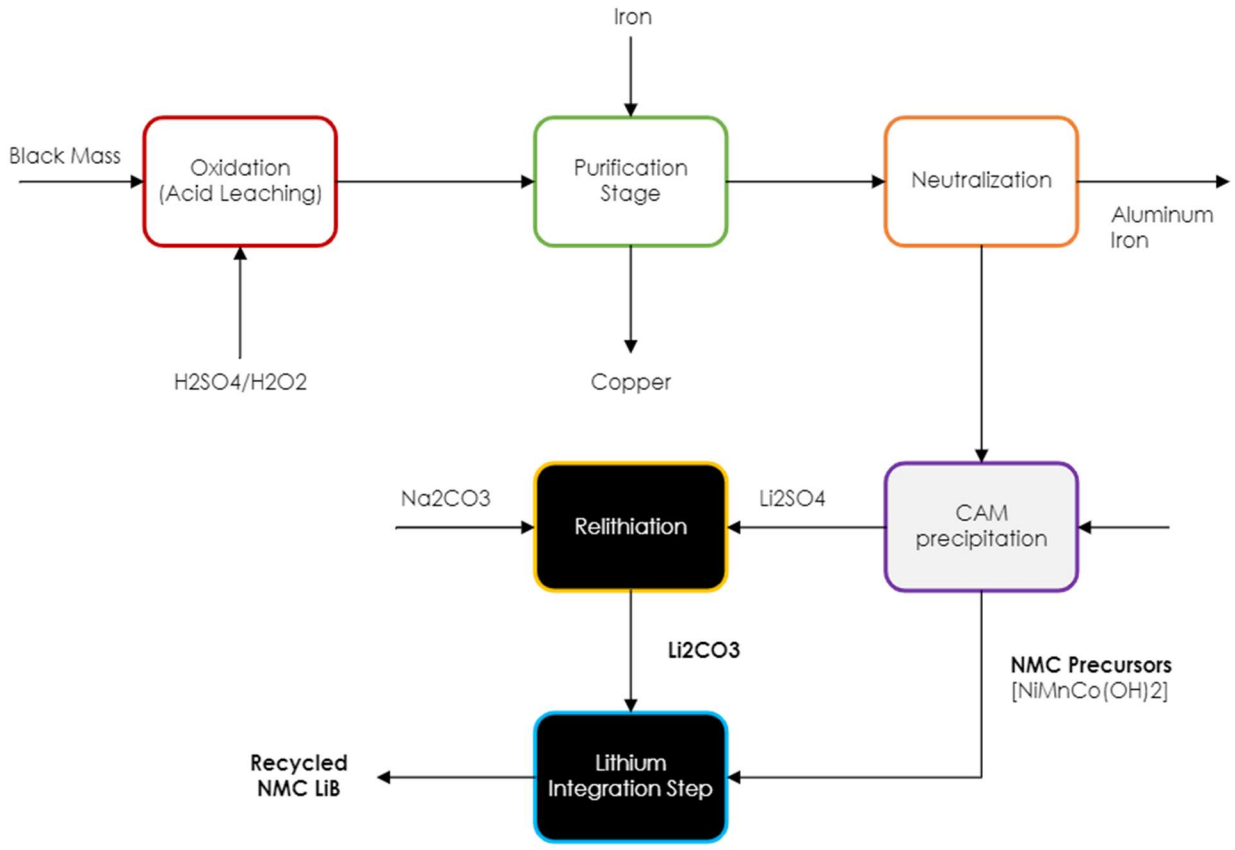

Figure 6. Process of Recycling NMC LiB

Hydrogen peroxide is added to control the electrochemical potential of the mixture to ensure the multivalent metals are in a certain oxidative state (+2, +3 and +2 for manganese, cobalt and nickel, respectively). This minimizes the loss of CAM as this prevents the precipitation of NMC as oxide/hydroxide salts. The addition of H_2O_2 has shown that the extraction of Co and Li increased from 40% and 75% to 85% for both metals. This can be explained by the

reduction of Co^{3+} to Co^{2+}, which is more easily extracted (Windisch-Kern et al., 2022). The same effect can be deduced to Ni and Mn metals, as well.

The Pourbaix diagrams of manganese and nickel are shown below in Figure 7 and Figure 8, respectively. The Pourbaix diagram illustrates the oxidation states of a metal with respect to the pH and redox potential. At certain combinations of pH and redox potential and with the presence of water and/or oxygen, it's possible that manganese can precipitate out as MnO_2 even in acidic conditions.

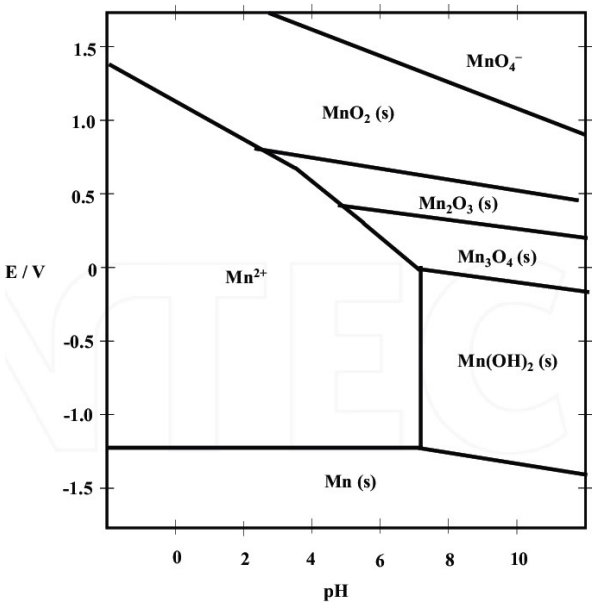

Figure 7. Pourbaix diagram of Manganese (Yi & Majid, 2018)

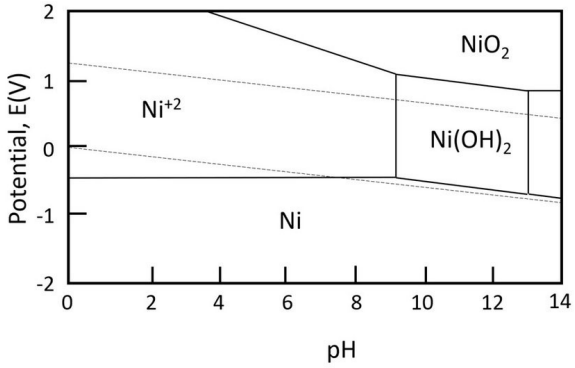

Figure 8. Pourbaix diagram of Nickel (Singh et al., 2020)

Thus, 30-50% hydrogen peroxide is added as a reducing agent to maintain the redox potential at a certain limit. In addition, H_2O_2 decomposes into water which does not cause more impurities in the mixture. After this process, what remains is a soluble solution of metals and graphite as the remaining solid (Latini et al., 2022). Variables in this step include the acid concentration, leaching time and the temperature. Optimal conditions are found at pH 3-4, 2.5 M H_2SO_4 and a liquid-to-solid ratio of 5 L acid/kg solids for 2 hours under 40°C heat (Garole et al., 2020).

The leachate contains the metals Co, Ni, Mn, Cu, Al, Li and Fe ions, with insoluble graphite removed via filtration. Metallic impurities (i.e., metals outside of Li-NMC) in the leachate are then removed via neutralization with 10% NaOH solution at 95°C for 2 hrs. At a pH level of 6-7, Fe, Al and Cu are precipitated out as hydroxides, leaving the Li-NMC in the solution (L. Chen et al., 2011).

At this point, stoichiometry adjustments are done by adding fresh $MnSO_4$, $CoSO_4$ and $NiSO_4$ on the filtrate to obtain the desired molar ratio according to the configuration of the NMC battery. The solution then undergoes the coprecipitation step to precipitate out nickel, manganese and cobalt as hydroxide salts. This serves as the transition metal precursor of the cathode active material, $Ni_xMn_yCo_{1-x-y}(OH)_2$.

In this process, sodium hydroxide mixed with ammonium hydroxide is added to achieve a pH of 11. At this pH level, nickel, manganese and cobalt exist as $Ni(OH)_2$, $Mn(OH)_2$ and $Co(OH)_2$, respectively based on their Pourbaix diagrams in figures Figure 7, Figure 8Figure 9. Ammonium hydroxide is added as a chelating agent and is also added to lower the cost associated with using NaOH, as well as lowering the sodium impurities in the solution – all while achieving the same pH level (Latini et al., 2022).

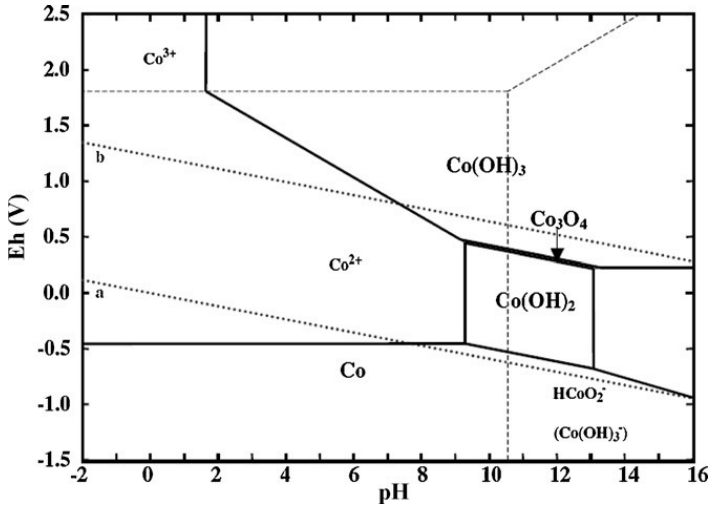

Figure 9. Pourbaix diagram of cobalt (Garcia et al., 2008)

Some lithium losses are also expected but the loss is at a minimum at this pH level. The mixture is stirred for 2 hrs at 50°C with constant N_2 bubbling to prevent oxidation of Mn^{2+} to Mn^{4+} (Latini et al., 2022). This operating condition is realized to all CAM components as it occurs in the manufacturing of virgin CAM materials.

The recovered lithium precursor is then mixed with the NMC hydroxide precursor, along with some virgin Li_2CO_3 to adjust to the right stoichiometry. Typically, the lithium is discarded in this process as purely fresh lithium carbonate is used. The molar ratio of Li to NMC is in the range of 1.0-1.1. The blended powders then undergo ball-milling for 48 hours and packed into pellets (Gratz et al., 2014). Lastly, the pellets are sintered at 900°C for 12-15 hrs to produce NMC with the choice of lithium source, oxidizing atmosphere and the lithiation step are the main operating conditions in this process.

Lithium Recovery

Precipitation

After filtering out the NMC hydroxide precipitates, the filtrate is only left with lithium, sodium, sulfate and hydroxide ions. Lithium is typically recovered via precipitation with sodium carbonate. The lithium and sulfate ions then undergo the following precipitation reaction:

$$Li_2SO_{4\,(aq)} + Na_2CO_{3\,(aq)} \leftrightarrow Li_2CO_{3\,(s)} + Na_2SO_{4\,(aq)}$$

Based on the solubility of these four salts, only lithium carbonate is highly insoluble. Taking into account the effect of temperature, the solubilities of Li_2SO_4, Na_2CO_3, Na_2SO_4 and Li_2CO_3 are illustrated in Figure 10 below. Starting at 40°C, the solubility of the salts drastically increases except for that of Li_2CO_3.

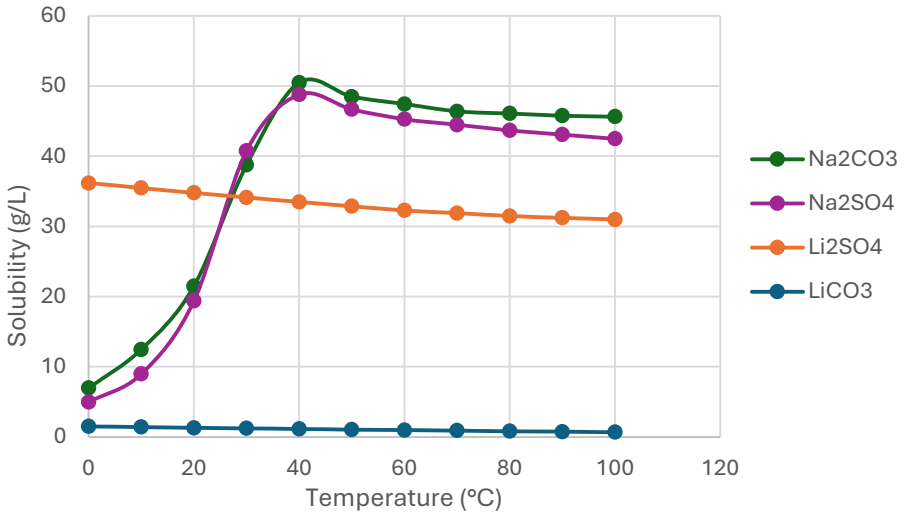

Figure 10. Solubility curve of some sodium and lithium salts

Operating conditions involved in this step include the initial lithium concentration, temperature, stoichiometric ratio of the added Na_2CO_3, and the reaction time. For this work, the effects of the temperature, stoichiometry and reaction time were investigated as these variables were varied as follows:

- Temperature: 50°C, 70°C, 90°C
- Stoichiometry: 110%, 120%, 200%
- Reaction time: 0.25 h, 0.5 h, 1 h, 2 h

For each combination of conditions, a 300-mL stock Li_2SO_4/Na_2SO_4 solution with added ammonium hydroxide (11% volume) was prepared to simulate the filtrate after the CAM precipitation step. This was done through dissolving 40 g of $Li_2SO_4 \bullet H_2O$ and 80 g Na_2SO_4 with

11 mL of 5.0 M NH_4OH in 1 L solution. The resulting initial lithium concentration was calculated to be 4.34 g/L. This parameter is kept constant across all runs.

Based on the stoichiometry, a set amount of solid Na_2CO_3 was added to solution when the set temperature is reached to facilitate the precipitation reaction. The reaction was done with constant stirring. The Li_2CO_3 precipitate was then recovered and dried 80°C overnight.

$$Recovery = 1 - \frac{V_{f,filtrate} \times [Li^+]_f}{V_{o,filtrate} \times [Li^+]_o}$$

$$Purity = 1 - \frac{MM_{Na2SO4} \times \%Na_f}{2MM_{Na}}$$

CO_2 Gas Absorption

A novel method of recovering lithium carbonate is by heterogeneous precipitation with carbon dioxide gas. The carbon dioxide dissolves in water forming carbonic acid. As an acid, H_2CO_3 undergoes dissociation where bicarbonate and carbonate ions are produced. The reactions go as follows:

$$CO_{2\,(g)} + H_2O_{\,(l)} \leftrightarrow H_2CO_{3\,(aq)}$$

$$H_2CO_{3\,(aq)} + H_2O_{\,(l)} \leftrightarrow H_3O^+_{\,(aq)} + HCO_3^-{}_{(aq)}$$

$$HCO_3^-{}_{(aq)} + H_2O_{\,(l)} \leftrightarrow H_3O^+_{\,(aq)} + CO_3^{2-}{}_{(aq)}$$

The carbonate ions then react to the lithium ions to form lithium carbonate.

$$2\,Li^+_{\,(aq)} + CO_3^{2-}{}_{(aq)} \leftrightarrow Li_2CO_{3\,(s)}$$

It is important to note that the input of CO_2 gas significantly lowers the pH due to the formation of carbonic acid. The concentration of bicarbonates and carbonates are heavily dependent on equilibrium conditions such as the concentration of hydronium ions (i.e., the pH). Figure 11 below shows the species composition of carbonic acid dissociation with respect to the pH.

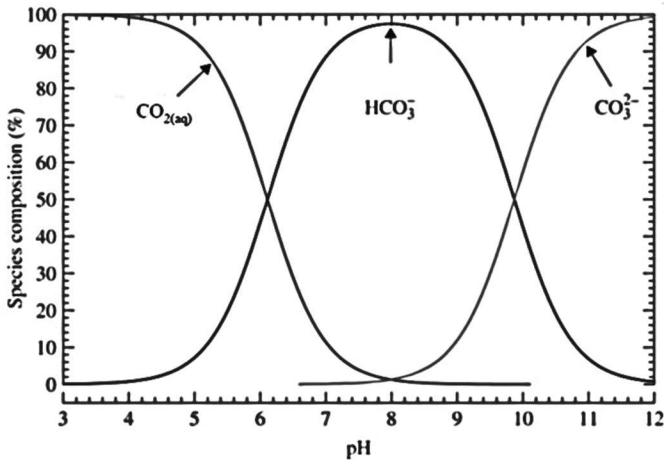

Figure 11. Equilibrium proportions of the carbonic acid system (Han et al., 2020)

The intersections of species curves signify the pKa of the dissociation constant. For example, pKa_2 signifies the pH at which there are equal parts carbonate and bicarbonate ions. A pH higher than pKa_2 means that carbonate ions are the dominant species. In the case of the carbonic acid system, this is equal to a pH of 10.3 (Han et al., 2020). Thus, the pH of the system needs to be controlled to allow the precipitation of Li_2CO_3 (Figure 12).

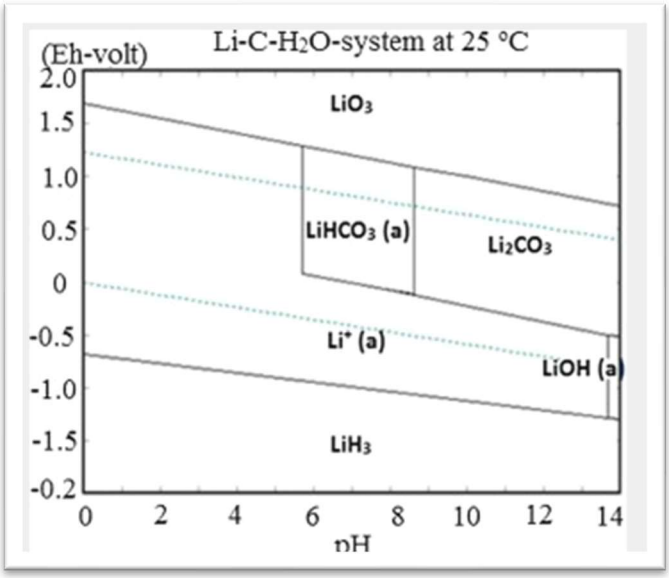

Figure 12. Pourbaix diagram of Li-H2O system

In this experiment, 700 mL of stock solution (a simulation of the filtrate after co-precipitation) was used with constant stirring (700 rpm) with consistent CO_2 bubbling at a set temperature for a set number of reaction time. Throughout the duration of the reaction, the pH of the system was controlled by periodically adding 4M NaOH solution to maintain the pH at around 10.5-10.8. The variables were identified to be the CO2 gas flow, temperature, and reaction time. These were varied as follows:

- Temperature: 70°C, 90°C
- CO_2 gas flow rate: 100 mL/min, 150 mL/min, 200 mL/min
- Reaction time: 1 h, 2 h, 3 h

Similarly to the precipitation experiment, the precipitates were recovered and dried at 80°C overnight.

Validation of Li_2CO_3

To evaluate the lithium recovery processes, factors associated with the processes' efficiency and cost-effectiveness were determined. This is mainly tied to the recovered precipitate's purity and the yield of the process. For the moment, while there is no set purity value for lithium carbonate precursors, the higher purity is associated with a higher quality and price. Meanwhile, the European commission has set a goal that by 2027, a 50% recovery (yield) rate is doable when recycling lithium carbonate.

In determining these factors, an Inductively Coupled Plasma Optical Emission spectroscopy (ICP-OES) analysis was conducted on the Li_2CO_3 precipitate and its filtrate. This was done by dissolving the specimen with 69% HNO_3 and diluting the solution in accordance with the operating concentration of the equipment. In addition, an X-ray Diffraction analysis was also done on the obtained solids to analyze the crystalline phases and structure of the obtained solid. It is also a way to qualitatively determine the presence of impurities.

Integration to NMC synthesis

A black mass was simulated where the CAM metal salts were precipitated out as hydroxides. The filtrate underwent precipitation using both methods of lithium recovery obtained at optimal conditions. The recovered lithium carbonate was pulverized along with the hydroxides of nickel, manganese and cobalt. The lithiation step was carried out in a muffle furnace in two phases: 500°C for 6 hours and then 850°C for 12 hours. In between phases, the samples were ground to disperse the particles and redistribute the particle size.

The first phase is carried out to combine the hydroxides of nickel, manganese and cobalt oxides where all salts have a melting point lower than lithium carbonate. This allows the hydroxide salts to mix below the melting point of the lithium precursor. The second phase allows the lithium carbonate to get linked with nickel, manganese and cobalt, forming $L_i(Ni_xMn_yCo_{1-x-y})O_2$. This process depends on the time, temperature, cooling and heating rate ramps because these parameters result to different morphologies.

Characterization of recycled Li-NMC

Electrochemical characterizations were assessed with respect to the as-recovered materials and to the pristine cathode materials conventionally used for commercial LiB. First, the lithiation product (active material) was mixed with Polyvinylidene fluoride (PVDF) binder and conductive carbon as the cathode material. The active material comprises 85% of the electrode material, with the balance equal parts PVDF and conductive carbon. A half-coin cell was prepared using lithium metal as the negative electrode. Then, cyclability tests was done to determine the capacity and voltage of the battery with increasing C-rates, along with the comparison to those of batteries made from pristine lithium carbonate.

Results and Discussion

Lithium Recovery

Precipitation with Sodium Carbonate

Figure 13 below shows the total lithium recovery with sodium carbonate. Total lithium recovery refers to the percentage of lithium recovered with respect to the total lithium present in the solution. As discussed in Figure 10, lithium carbonate has a low solubility relative to other salts in the solution with around 1 g/L. This implies that it is impossible to recover all the lithium ions in the solution at any given temperature.

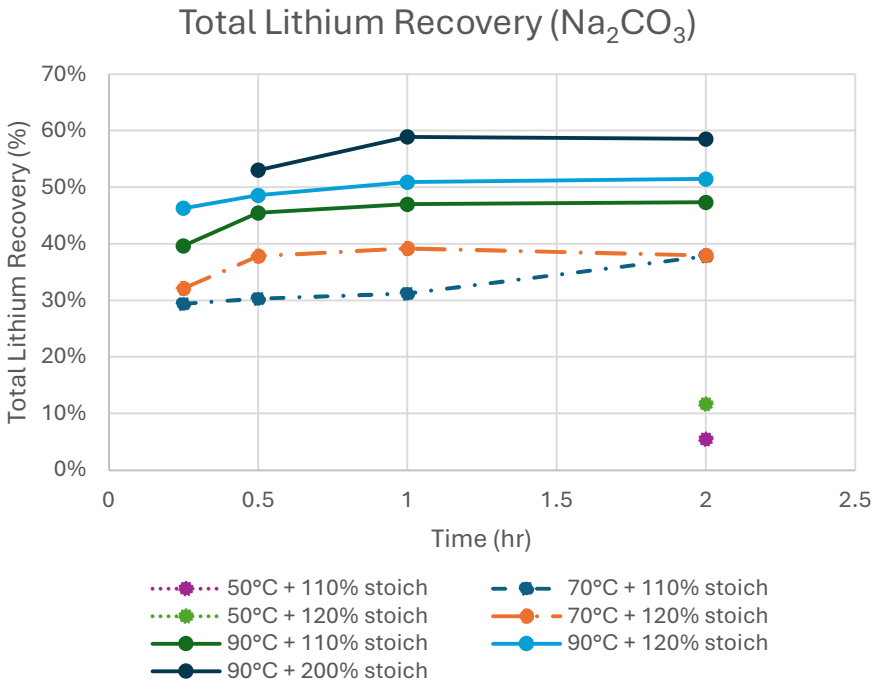

Figure 13. Total Lithium Recovery using sodium carbonate precipitation

The results show an increase in yield with respect to reaction time and temperature. The temperature effect corresponds to the decrease in solubility of lithium, while the time effect is mostly related to the kinetics of the reaction which allows the progression of the precipitation reaction.

The purity of the recovered salt at different operating conditions is shown in Figure 14 below. The temperature had a positive effect on the purity of the solid. This was attributed to the reduced amount of filtrate residue during the filtration process. The reaction time had an opposite effect as a longer time allows for the side reactions to progress, thus allowing the

formation of more sodium sulfate. Maximum quality was reached at 1 hour and 90°C with 98.36% purity using 110% Na_2CO_3 stoichiometry.

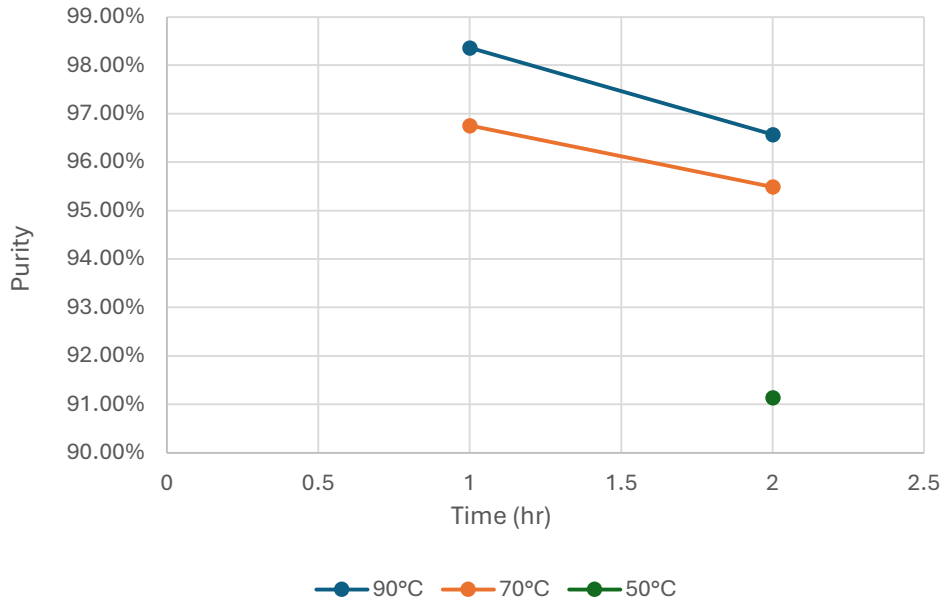

Figure 14.Li_2CO_3 Purity using sodium carbonate precipitation

Based on Figure 15 below, the dosage of sodium carbonate provides a positive effect on the lithium recovery, but the opposite trend was observed in the purity of the product necessary for the battery market.

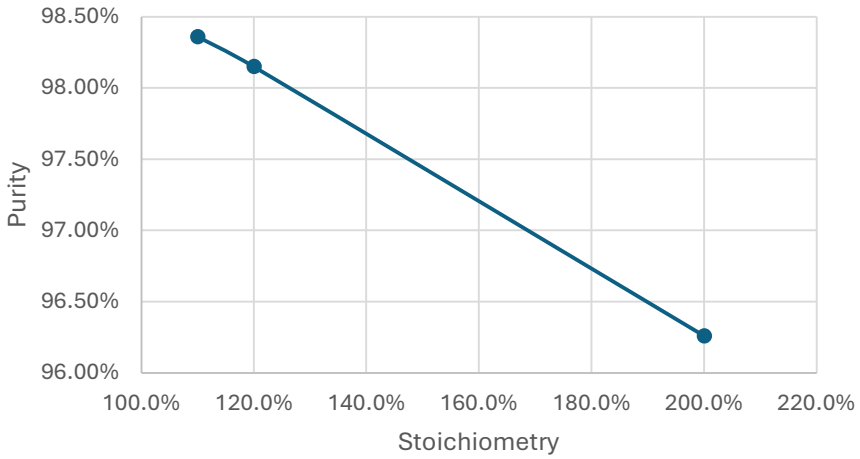

Figure 15. Effect of the Na2CO3 loading on purity

Considering both lithium carbonate recovery and purity, the optimal temperature and time was found to be 90°C and 1 hour, respectively. Meanwhile, there is also an increasing trend with regards to the excess stoichiometry of added Na_2CO_3, but it remains to be seen with more stoichiometry levels to determine an optimal point.

Precipitation with Carbon Dioxide

Figure 16 below shows the change of pH through time with constant CO_2 flow. By around 40 minutes, the system reaches equilibrium with an acidic pH. This implies that the carbonate ions exist as carbonic acid, which would then dissociate into bicarbonate and carbonate ions. The increase of the temperature reduces the CO_2 absorption capacity of the liquor, but it increases the kinetics of the reaction.

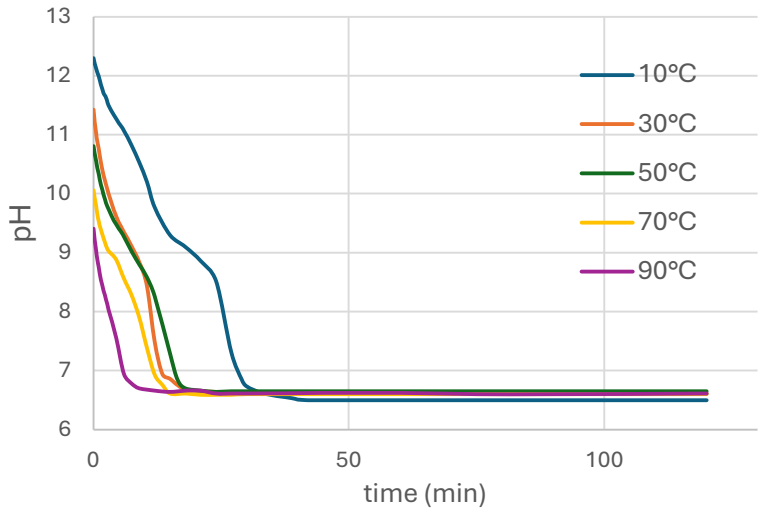

Figure 16. CO_2 absorption in the filtrate

At acidic pH levels, the dominant species is carbonic acid where there is little to no dissociation between bicarbonate and carbonate ions. At near neutral pH levels, the bicarbonate ion is dominant, but $LiHCO_3$ is highly soluble so no precipitation reaction would take place.

Thus, there is a need to increase the pH such that the dominant species is CO_3^{2-}. This is done by intermittently adding NaOH to maintain the pH above the pKa_2 (around 10.3-10.5) of carbonic acid. Table 4 below shows the NaOH consumption at 90°C, along with the combination of carbon dioxide flow and the reaction time.

Table 4. NaOH addition for pH adjustement

CO2 Flow (mL/min)	Time (h)	Vol NaOH 4 M (mL)
100	1	91
	2	125
	3	125
150	1	93
	2	175
	3	199
200	1	129
	2	212
	3	313

Figure 17 below shows the total lithium recovery with carbon dioxide. The results show a similar trend with respect to reaction time and temperature. The temperature effect corresponds to the decrease in solubility of lithium, while the time effect is mostly related to the kinetics of the reaction which allows the progression of the precipitation reaction.

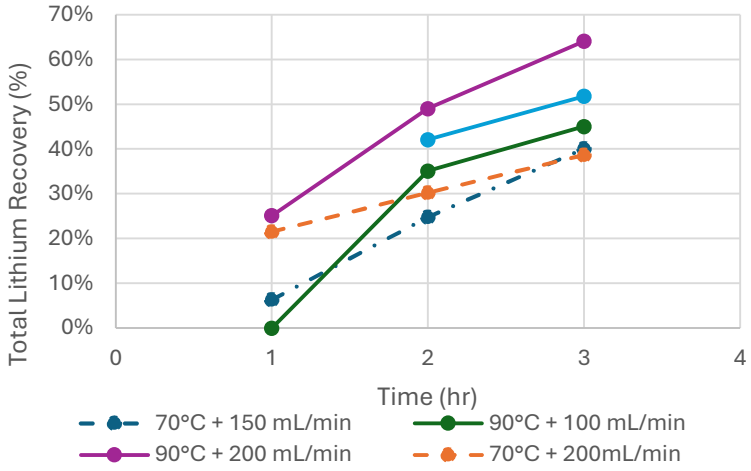

Figure 17. Total Lithium Recovery using carbon dioxide absorption

Maximum recovery was reached at 90°C, 200 mL/min and 3 hours reaction time with 64.12%. This corresponds to 97.12% of the recoverable lithium carbonate in the solution. In terms of reaction time, there does not seem to be an optimal point so a need to see the effects of reaction times beyond 3 hours. The recovery values obtained from this method are observed to be larger. This can be attributed to the higher amount of CO_3^{2-} ions from the CO_2 gas as the gas is continuously absorbed throughout it.

The purity of the recovered salt is shown in Figure 18 below. The trend is the same in terms of the effect in temperature and reaction time. Maximum quality was reached at 2 hours, 200 mL/min and 90°C with 97.10% purity. This is slightly lower than the purity obtained using precipitation with Na_2CO_3. This is due to the impurities introduced by the addition of NaOH, where the increase of sodium ions promotes the precipitation of sodium sulfate.

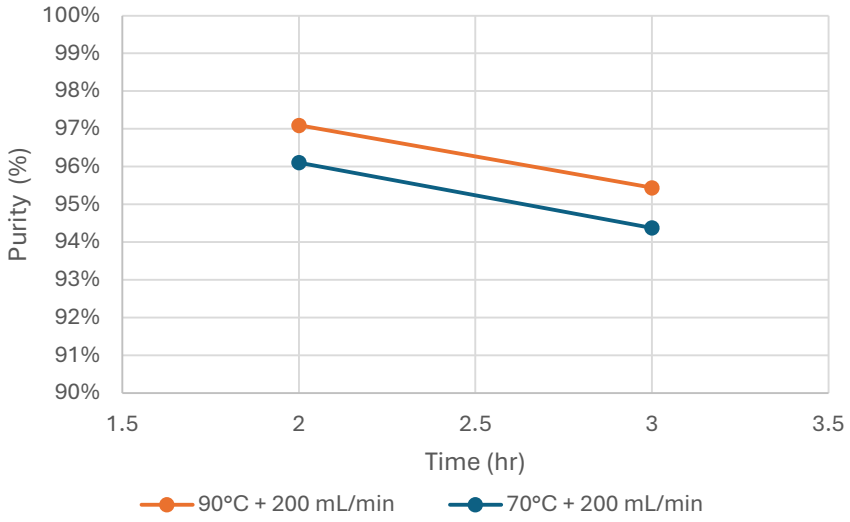

Figure 18.Li_2CO_3 Purity using carbon dioxide absorption

Table 5 below shows the summary of the optimal optimization part of the study, and the corresponding process variables obtained under these conditions.

Table 5. Optimal process conditions for lithium recovery.

	Li_2CO_3 from Na_2CO_3 precipitation	**Li_2CO_3 from CO_2 precipitation**
Optimal Temperature (°C)	90	90
Optimal Time (h)	1	3
Optimal Loading	120 %	200 mL/min
Recovery (%)	50.91	64.12
Purity (%Li_2CO_3)	97.1	96.7
Na (%)	0.94	1.07
Ni (ppm)	107	107
Mn (ppm)	44	44
Co (ppm)	31	17

Parametric studies by Zhao et al. (2019) show that the initial lithium concentration has an increasing effect on the lithium recovery rate, while the quality of Li_2CO_3 recovered is

decreasing, as shown in Figure 19Figure 20. This signifies the need to optimize this parameter into getting the optimal concentration to obtain high recovery and purity.

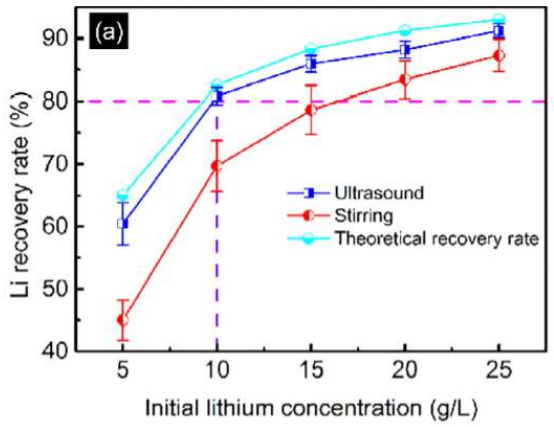

Figure 19. Effect of initial lithium concentration on lithium recovery (Zhao et al., 2019)

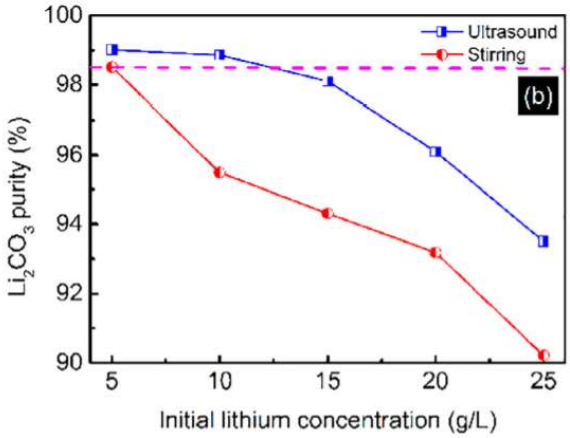

Figure 20. Effect of initial lithium concentration on precipitate purity (Zhao et al., 2019)

From 5 to 25 g/L of Li^+, it was found that a lithium concentration of 10 g/L is optimal to achieve high recovery and purity. Ultrasonification was also incorporated into the precipitation step which significantly improved the process, although this also reduced the particle size of the Li_2CO_3 powder as shown in Figure 21 below.

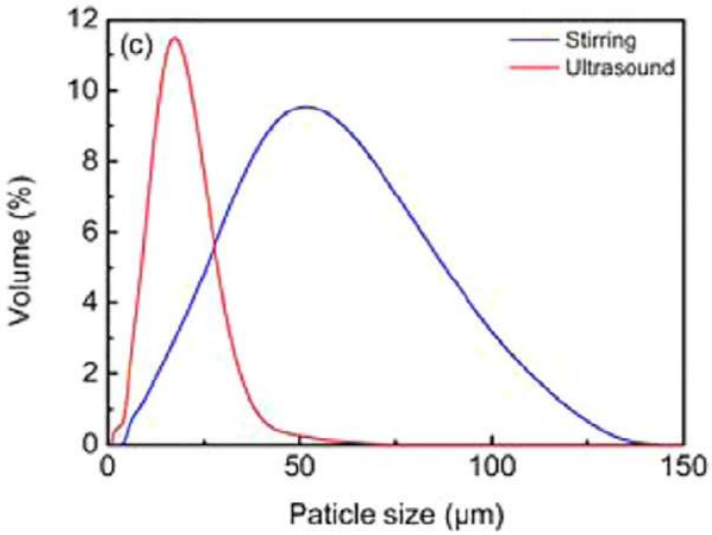

Figure 21. Particle size effects on the presence of ultrasound in the precipitation process (Zhao et al., 2019)

Characterization of Recycled Battery Materials

While the accelerating demand of lithium-ion batteries calls for the need of recycling to reduce the pressure in the battery supply chain, there are concerns regarding the reintroduction of spent LiB to the supply chain. Questions arise about the recycled LiB's ability to compete in the market in terms of cost, yield and performance. The academia and industry have made efforts to optimize the battery recycling process to improve the cost and yield of recycled batteries, as well as preparing the process ready for mass production. In terms of the electrochemical performance, impurities are thought to be introduced in the recycling process along with the complex structure of LiBs. This calls for the verification and testing for the electrochemical performance of recycled batteries (Ma et al., 2021).

Characterization methods such as Scanning Electron Microscopy (SEM) and X-Ray Diffraction (XRD) were used to observe the morphology and structure of the recycled battery. For this study, the recycled particles ($Li_{1.009}Ni_{0.65}Mn_{0.17}Co_{0.16}O_2$) are compared to a control powder with commercial battery-grade lithium carbonate.

XRD Analysis

XRD analysis was conducted on the recovered Li_2CO_3 mainly to check for impurities and the identification of these impurities. Figure 22 below shows the XRD graph of a recovered Li_2CO_3. The figure confirms the presence of sodium sulfate in the precipitate as the main impurity in the solid sample.

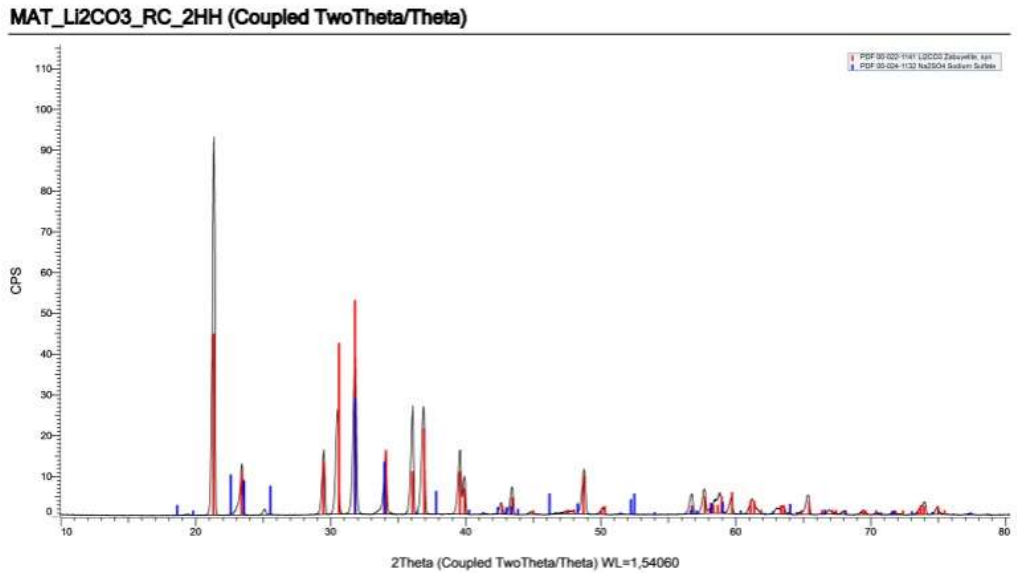

Figure 22. X-ray Diffraction (XRD) of recovered Li_2CO_3

In a similar study, Ma et al. (2021) developed a scalable closed-loop battery recycling process that combines hydrometallurgical and direct recycling benefits. the XRD patterns match the recycled and control powders, providing a good degree of crystallinity. Recycled particles show a lower degree of cation mixing of Li^{+}/Ni^{2+}. Cation mixing affects the electrochemical performance of layered cathode materials as it is associated with lower battery capacity due to losses of Li active sites (Li et al., 2023).

SEM Imaging

SEM images of the lithium carbonate samples are shown below in Figure 23 and Figure 24 for the commercial and recycled salts. Observations from SEM show that the recycled battery powder exhibits a similar morphology as the control material. It was noted, however, that the recycled battery powder has a slightly larger crystal size distribution, especially in the center of the particle. This lowers the tap density and increases the surface area of the recycled particles, as well as helps in buffering the strain and deformation. This property mitigates capacity fading during battery cycling (Ma et al., 2021).

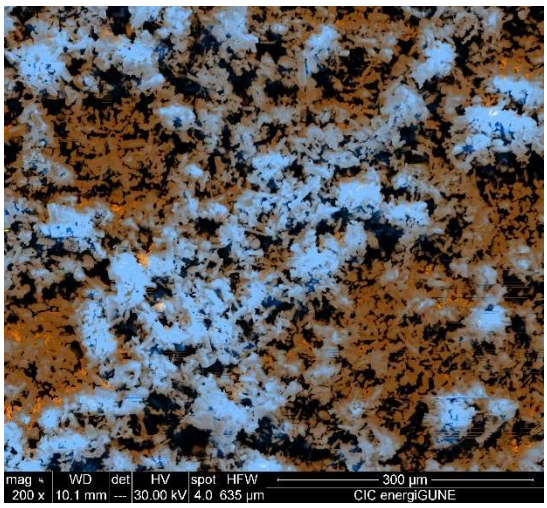

Figure 23. SEM Image of Commercial Li_2CO_3 (400x magnification)

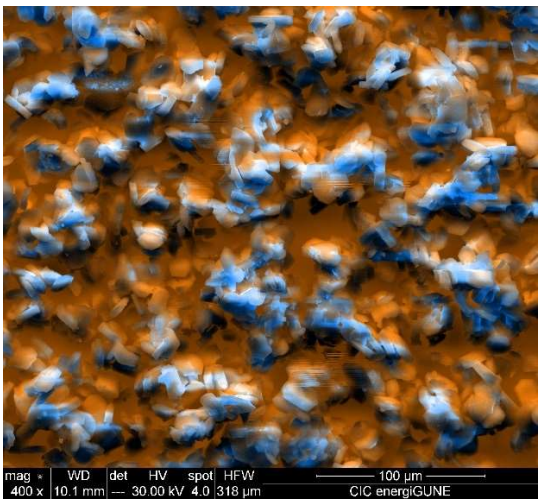

Figure 24.SEM Image of Recycled Li_2CO_3 from Na_2CO_3 (400x magnification)

The lithiation products using the Li_2CO_3 samples are shown Figure 25 and Figure 26. The lithiated NMC particles in both samples have similar sizes and particle distribution, with the agglomerates being attributed to the presence of co-precipitated nickel, manages and cobalt hydroxides. These hydroxides stem from the completeness of the lithiation reaction.

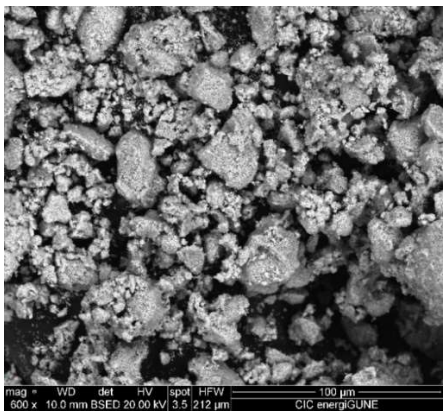

Figure 25.SEM Image of lithiated NMC with commercial Li_2CO_3 (600x magnification)

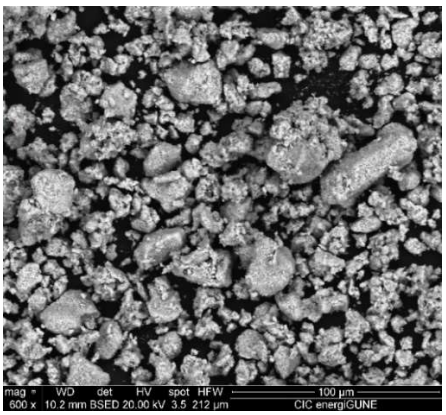

Figure 26. SEM Image of lithiated NMC with recycled Li_2CO_3 from Na_2CO_3 (600x magnification)

In general, there seems to be no noticeable difference between the morphology and size of the lithiation products with respect to the morphology of Li_2CO_3 particles. This implies that any potential difference in the electrochemical properties of lithiated NMC samples can be only attributed to the composition of the material – that is, the impurities present in the precipitate. Similarly, the morphology of the NMC-cathode is shown below in Figure 27 and Figure 28.

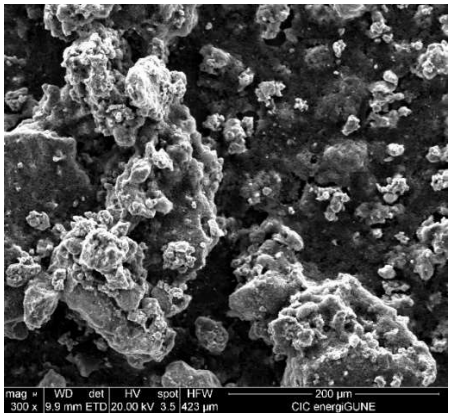

Figure 27. SEM Image of NMC cathode with commercial Li2CO3 (300x magnification)

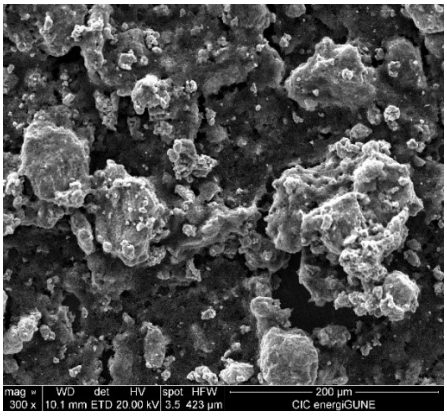

Figure 28. SEM Image of NMC cathode with recycled Li2CO3 (300x magnification)

Electrochemical Testing

Battery testing methods need to be performed considering the possibility of upscaling to be reliable and translatable into the industry for commercial applications. In this study, the testing is associated with coin cells. Figure 29 below shows the battery cycling tests for the LiB from recycled Na_2CO_3.

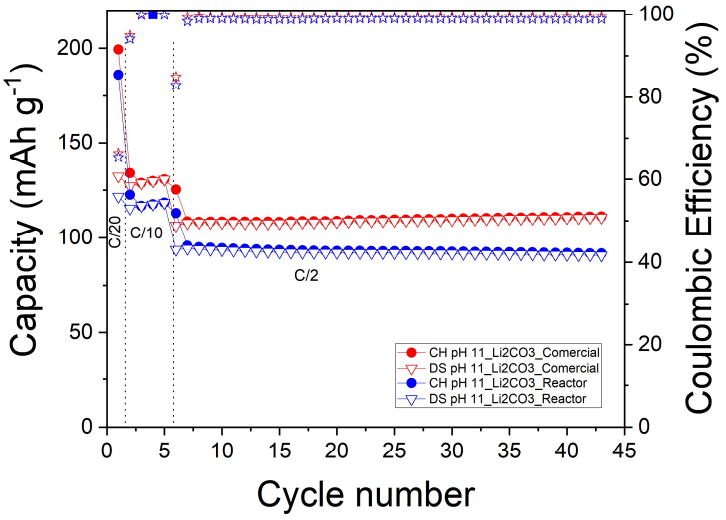

Figure 29. Cycling test of Recycled LiB with Na_2CO_3

In both cases, the recycled components were compared against the control of pristine commercial Li_2CO_3. In the case of the recycled LiB with Na_2CO_3, the obtained capacity after the first discharge was 122 mAh/g at a C-rate of C/20, compared to 132 mAh/g of the control. This corresponds to 70% and 75% of the theoretical capacity of Li-NMC, respectively. This gap from the theoretical capacity is attributed to the irreversibility of the components in the battery, as well as some physical limitations in the method of preparation (e.g., manual grinding of the active material resulting to a less uniform particle size distribution).

Throughout the cycling of the battery, the battery has also exhibited stability in terms of its capacity and voltage. Based on capacity measurements, the specific capacity of the recycled battery with Na_2CO_3 has decreased to 90.9 mAh/g after 40 cycles from 94.1 mAh/g in the first cycle. The coulombic efficiency was measured to be 99.7% at this cycle. This value refers to the ratio of the energy released after the full charge, with respect to the charging capacity in the same cycle. Measurements also show that the coulombic efficiency is stable even in later cycles.

Error! Reference source not found. shows the voltage with respect to the capacity throughout cycling of the recycled batteries using Na_2CO_3. There is a noticeable decrease in the capacity with respect to the voltage in between the 5th cycle and the 10th cycle. From the measurements in the same figure, this change occurred somewhere in the 7th cycle. There is

also a significant drop after the first cycle, which is associated with the formation of the Solid Electrolyte Interface (SEI). Thus, this later decrease can be attributed to further irreversible interactions in the system.

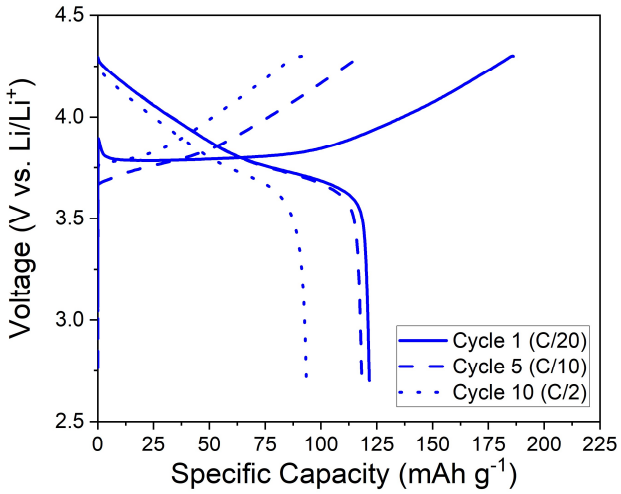

Figure 30. Change in Voltage of Recycled LiB (Na2CO3)

Due to time constraints, this is the only electrochemical test performed with the recycled NMC battery. The United States Advanced Battery Consortium (USABC) PHEV protocol could be followed to have a more complete picture of the battery's mechanical and electrochemical properties. These tests evaluate properties like self-discharge, energy density, cold resistance, calendar life and degradation mechanism of the battery.

For example, nanoindentation can be performed to measure mechanical performance. Ma et al. (2021) tested recycled NMC powders by applying compressive force and measuring the mechanical deformation of the powders. Control powders had shown to be able to withstand more compressive pressure, but the recycled powders can withstand twice the amount of compressive strain than the control powder. This makes the recycled powders less brittle than the control powders, along with a lower elastic. This makes the recycled battery more resistant to repetitive deformation during the charge-discharge cycle.

Industrial tests such as cold crank test, hybrid pulse power characterization (HPPC) and calendar life were conducted to evaluate the ability of the batteries to stresses in load and temperature. The cold crank test simulates low-temperature conditions and measures the voltage threshold of the battery at -30°C and state of charge (SOC). From the test conducted, it was shown that the recycled and controlled materials can sustain above the 2.2V voltage threshold after 3 consecutive discharge pulses. However, the recycled battery has a slightly higher resistance than the control powder (Ma et al., 2021).

Meanwhile, the calendar life simulates the minimal usage of the battery where a fast degradation is established at 50°C to accelerate the decay process. This property is

measured through cycle life testing where the battery is charged and discharged at a certain voltage range and a specific discharge rate until the capacity retention rate is at 70%. Figure 31 shows the calendar life of the recycled and control batteries from the cycling test at 2.7-4.15 V at a discharge rate of 1C. It was shown that the recycled battery materials have a cycle life of 4200 cycles before reaching 80% capacity retention, while it would take another 7400 more life cycles to drop to 70% capacity. Under the same conditions, the control battery took 3150 cycles and 4450 more cycles to reach 70% and 80% capacity, respectively (Ma et al., 2021).

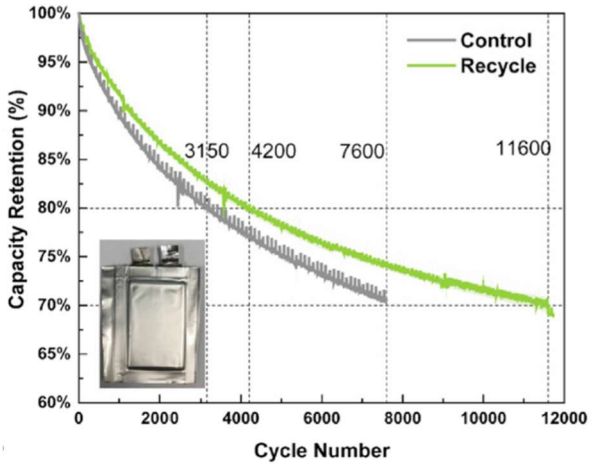

Figure 31. Cycle Life Testing (Ma et al., 2021)

From the electrochemical testing, it shows that the recycled battery is comparable to batteries using pristine lithium carbonate. Impurities in the NMC precursors explain the gaps in the electrochemical properties of the coin cells from recycled materials. Sodium sulfate is the main impurity in the lithium precursor while for NMC hydroxides, lithium ions comprise the main impurity.

In an industrial scale, more impurities are present such as the aluminum and copper current collectors, as well as the iron casing of batteries. This highlights the importance of optimizing the conditions of the upstream processes as this carries over to the quality of the product. It is also possible to add more purification steps in the downstream process to improve the quality of the Li-NMC precursors before assembling them into a battery. In either case, this would increase the operational cost of the recycling plant. With ongoing improvements in the process of hydrometallurgical recycling, this indicates a promising outlook for the usage of recycled materials in the battery supply chain.

Economic Analysis

Scale-up process

An industrial scale was considered to assess the economic potential of adding a lithium recovery step in a recycling plant. A basis was set based on the amount of black mass processed annually. Two scenarios were compared with respect to the precipitating agent of the lithium carbonate precipitation. These scenarios dictate the residence time of the reactor, which is based on the optimal conditions obtained from the recovery experiments.

Table 6. Design Specifications of the lithium recovery unit of the hydrometallurgical recycling process

	Scenario 1	**Scenario 2**
Precipitating agent	Na_2CO_3	CO_2
Annual black mass processing, t/y	8500	8500
Annual Li_2SO_4 processing, t/y	1987	1987
Daily Li_2SO_4 processing, kg/d	5444	5444
Daily filtrate processing, /d	136	136
Reaction Time, hr	1	3
Reactant volume, m	5.67	18.9
Batches per day	24	8

Table 6 above shows the outline of the material flow in each scenario. The residence times used were 1 hour and 3 hours for the Na_2CO_3 and CO_2 scenarios, respectively. This corresponds to the difference in the size of the batch reactors and in turn, this will affect the heat and power requirements of the unit process. Since the precipitation with CO_2 needs a longer reaction time, a larger reactor volume is needed. This also means that there would be less batches to have the same amount of feed processed.

Table 7. Design Specifications of the reactor tank

	Scenario 1	**Scenario 2**
Precipitating agent	Na_2CO_3	CO_2
Liquid Volume, m^3	5.67	17.01
Tank Volume, m^3	6.30	18.90
Tank Diameter, m	1.37	1.97
Allowable Stress Design, psi	20000	20000
Allowable Stress Test, psi	22500	22500
Reactor thickness, mm	1.8	2.0
Stirring speed, rpm	600	700
Insulator thickness, mm	6	6
Corrosion allowance, mm	1.6	1.6

The heating requirement mainly refers to the amount of heat needed to obtain and maintain the operating temperature from the conductive and convective losses. The heat losses were then calculated using design equations of a tank, with the following material and design specifications. A A283M grade C carbon steel was arbitrarily used, as the system is not pressurized. In addition, fiber glass was designed to be the reactor insulator. Considering this material selection, the design specifications are shown above in Table 7.

The heat required to raise the temperature is calculated through the sensible heat of the solution. The liquid properties were estimated to be the same as that of water due to the dilute concentration of lithium sulfate in the solution. For each temperature condition, the sensible heat was calculated using the equation below

$$E_{sens} = V_{liq}\rho_{liq}C_{p,liq}\Delta T \qquad \textit{Equation 1}$$

Meanwhile, heat input is needed throughout the reaction time to maintain the temperature to a set level. This heat loss can be quantified with conductive and heat losses of the reactor tank due to the temperature difference with the environment with an assumed temperature of 25°C. Equation 2 and Equation 3 below show the calculation of the convective and conductive heat transfer losses.

Equation 2

$$E_{loss} = UA\Delta Tt$$

Equation 3

$$U = \frac{1}{\frac{d_o}{d_i} \times \frac{1}{h_i} + \frac{d_o\left(ln\,\frac{d_m}{d_i}\right)}{2k_{steel}} + \frac{d_o\left(ln\,\frac{d_o}{d_m}\right)}{2k_{fg}} + \frac{1}{h_o}}$$

where

d_i = Inner diameter of reactor tank
d_m = Outer diameter of reactor tank
d_o = d_m + insulator thickness
h_i = inner convective heat transfer coefficient
h_o = outer convective heat transfer coefficient
k_{steel} = Reactor conductive heat transfer coefficient
K_{fg} = Insulator conductive heat transfer coefficient

The heat loss is calculated with the heat transfer parameters estimated using liquid properties of water at the operating temperatures. Figure 32 and Figure 33 show the calculated heating requirements of the batch reactor. The heat requirement refers to the total heat required from the sensible heat and compensating the heat losses.

Equation 4

$$E_{requirement} = E_{sens} + E_{loss}$$

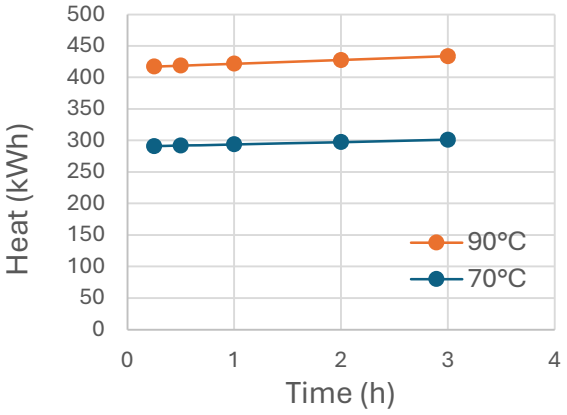

Figure 32. Heating Requirement for the Precipitation with Na_2CO_3

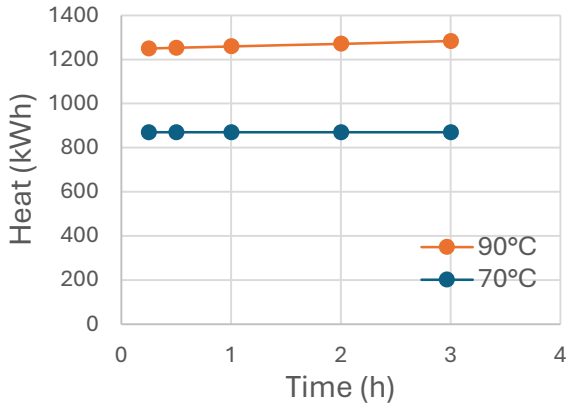

Figure 33. Heating Requirement for the Precipitation with CO_2

As expected, higher heating needs to be maintained at 90°C due to the higher temperature difference between the system and the environment. The slight increase is attributed to the reaction time as more heat is lost through convection through time. The larger heat requirement in the precipitation with CO_2 is due to the higher processed volume per batch.

Meanwhile, the power requirement refers to the impeller power used to stir the solution throughout the reaction. Arbitrarily, a Rushton turbine was selected for the impeller design which dictates the power number of the impeller. At turbulent conditions, the power number (N_p) approaches 2.5. Equation 5 shows the calculation for the impeller power, with the fluid properties estimated as that of water.

Equation 5

$$W = tN_p\rho N^3 {D_i}^5$$

where

t = Time
N_p = Power number (= 2.5)
ρ = Liquid density
N = Impeller speed
D_i = Impeller diameter (= $d_i/3$)

Figure 34 and Figure 35 show the different power requirements per batch with respect to the reaction time. At constant volume and impeller speed, there is a linear trend as the reaction

time is linearly proportional to the power requirement. The temperature affects the density of the fluid, but the density difference is not high enough to make a significant difference in the power requirement. In addition, the higher power requirement of the impeller is higher in the CO_2-Li_2SO_4 due to the size of the reactor.

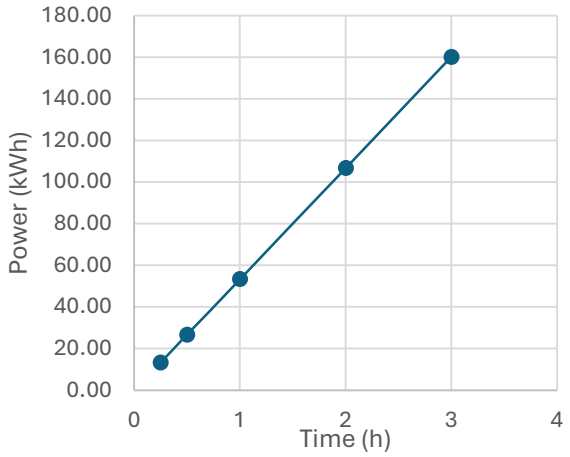

Figure 34. Power Requirement for the Precipitation with Na_2CO_3 at 90°C

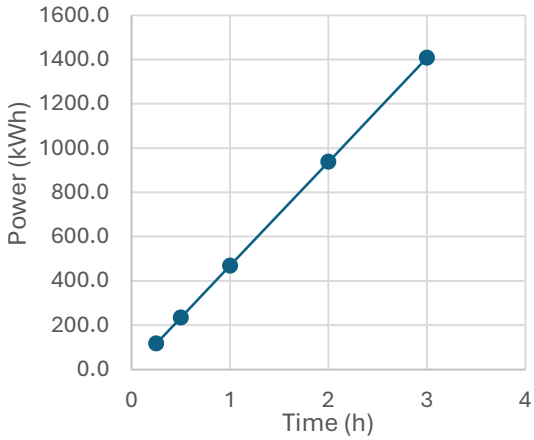

Figure 35. Power Requirement for the Precipitation with CO_2 at 90°C

OPEX Calculation

Pictured in Figure 36 below shows the unit operations involved in the added lithium recovery step. Both scenarios involve the precipitation reactor, press filter and the drying equipment. In the case of CO_2 precipitation, a mixer is involved due to the addition of NaOH to the material flow of the process. Normally, concentrated NaOH (around 50% NaOH) is readily available. To match the specifications in the process, a mixing operation is needed to obtain the designated concentration.

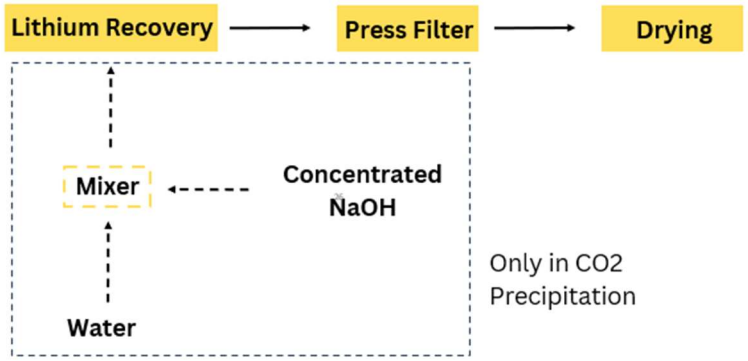

Figure 36. Operations in the added lithium recovery process

Table 8 below shows the factors considered for the OPEX components, along with their corresponding cost and benefits. In this analysis, only the Li_2CO_3 is considered as the source of income, whereas the Li_2CO_3 is considered as a battery-grade product. Using the difference of the operational costs and the income, the plant with Na_2CO_3 precipitation shows a much lower operating cost than that of CO_2 precipitation. This is due to the additional reactant (NaOH), as well as units of operation in the plant. On the other hand, the increased recovery of CO_2 precipitation increases the income significantly.

Table 8. OPEX Calculations for Spain

	Scenario 1	**Scenario 2**
	Na_2CO_3 Precipitation	**CO_2 Precipitation**
Operational Costs		
Power Requirement	€ 71,947.58	€ 869,377.35
Heating Requirement	€ 206,124.07	€ 210,187.08
Na_2CO_3 Cost	€ 156,388.88	
CO_2 Cost		€ 961,141.03
Water Usage		€ 15,335.24
NaOH Usage		€ 2,432,301.69
Manpower	€ 215,496.00	€ 215,496.00
Total Cost	€ 649,956.52	€ 4,703,838.39
Incomes		
Product Price	€ 8,939,307.05	€ 11,257,773.36
Net OPEX	**€ 8,289,350.53**	**€ 6,553,934.97**

Comparing the two scenarios, the precipitation with CO_2 gas shows a higher power requirement due to the higher volume used in the operation. The net OPEX is also higher due to the presence of other reagents like NaOH and water. To lower the cost of this process, more concentrated NaOH can be used to reduce the water usage and minimize the volume of the solution. In addition, carbon dioxide from a point source such as flue gas can be used to save on CO_2 cost and lower the carbon footprint. Applying these steps can potentially make precipitation with CO_2 more economically competitive.

The cost (OPEX) of the additional lithium recovery unit varies by country. This is due to the differences in the cost of electricity, gas, water and even chemicals in the territory. The differences are attributed to the countries' energy mix and economy. For example, countries with a higher proportion of renewable energy have lower cost of electricity. In this study, the operational cost was compared with countries like Italy, Sweden and Norway as shown in Figure 37 and Figure 38 below.

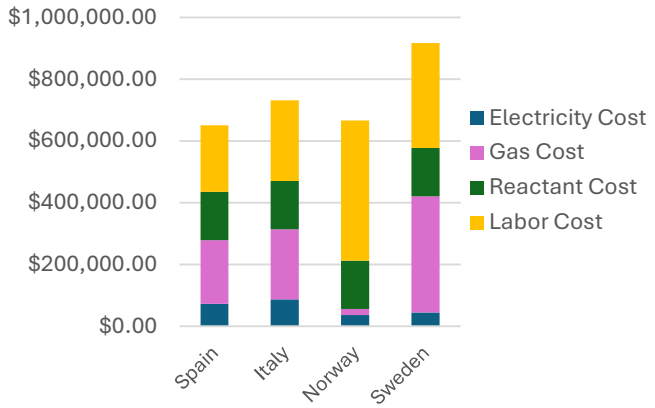

Figure 37. Cost comparison of the lithium recovery using Na_2CO_3

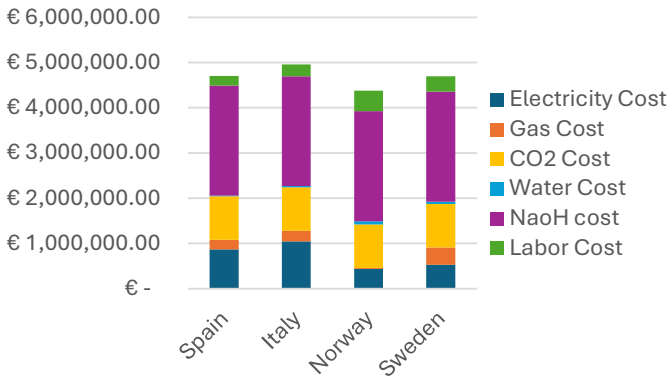

Figure 38. Cost comparison of the lithium recovery using CO2

For the recovery unit using Na_2CO_3, the countries compared show variable costs, especially in the labor cost. This is due to the stark difference between the hourly wages between Southern (Spain, Italy) and Northern (Sweden, Norway) European countries. It is also worth noting that being a gas exporter, the cost of gas in Norway is the lowest. This significantly drives down the cost that it is less costly to operate a lithium recovery unit in Norway than in Italy.

Meanwhile, the recovery unit using CO_2 shows a less variable cost due to the costs of the reactant (CO_2) and NaOH. Across all countries, the NaOH cost comprises most of the operating costs, with the cost of CO_2 coming in second. This also explains the large difference between the recovery unit using Na_2CO_3 and CO_2.

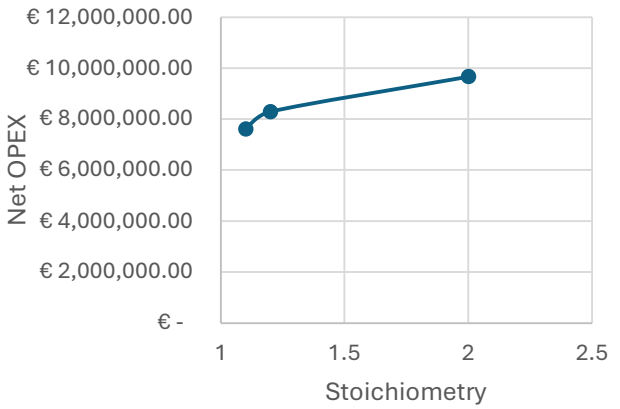

Figure 39. Net OPEX with respect to Na_2CO_3 stoichiometry

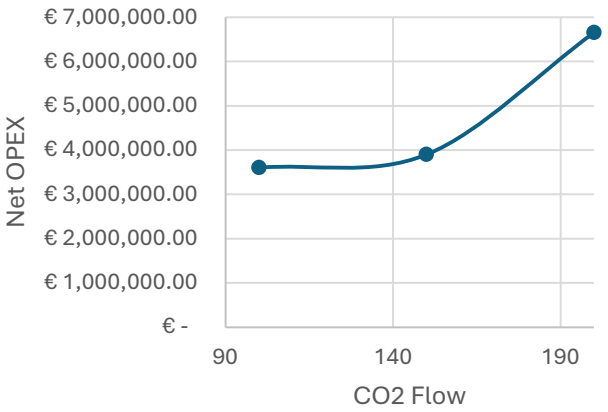

Figure 40. Net OPEX with respect to CO2 flow

Figure 39 and Figure 40 above show the changes in the Net OPEX (Incomes – Costs) with respect to the change of reactant input. The costs were obtained at the optimal temperature and reaction time. Using the corresponding recovery rate and energy requirement, the costs

were calculated at varying loading. Conditions outside the optimal loading are less profitable to a significant degree. While there is less cost associated with lower loading, the recovery is low enough that the income does not compensate enough. In contrast, higher loadings require more energy, but the higher recovery of lithium carbonate is high enough that the net OPEX is higher.

In addition, higher recovery of Li_2CO_3 through increasing the precipitant loading implies a reduction in purity, and consequently, in the product price. The net OPEX variation can provide the assumable cost of the additional Li_2CO_3 purification step.

Impact Analysis on Battery Recycling (Literature Study)

Discarded batteries pose risks to the environment and mineral resources. Recycling allows the reintroduction of spent batteries to the battery supply chain, prolonging their lifetime and maintaining their value. This has a direct influence on the emissions emitted throughout the battery's life. Thus, recycling LiB is not only important from an economic perspective, but it is also crucial for the sustainability of the new energy industries where LiB are important (e.g. EV industry, electronics, etc.).

Yang et al. (2024) performed a life cycle analysis (LCA) on spent LiB from EV, evaluating impact assessment categories such as global warming potential (GWP). Figure 41 below shows the comparison of net GWP associated with the battery recycling methods. While the recovery of EoL materials has negative impacts on the GWP, the recycling processes themselves generate emissions.

The net impacts on GWP, therefore, varies across the recycling methods due to the differences in techniques and technologies used. For example, the pyrometallurgical method of recycling has a very high energy requirement and lower recovery of materials. Thus, the net impact of the pyrometallurgical method is less negative than those of other recycling routes.

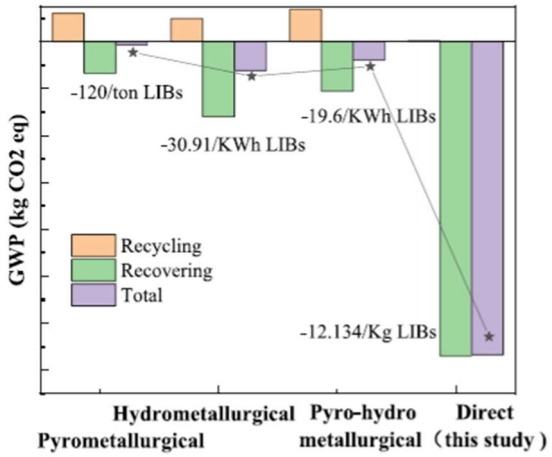

Figure 41. GWP associated with battery recycling methods (Yang et al., 2024).

Meanwhile, Figure 42 below illustrates the contribution of the battery components to the GWP based on 1 kg of recycled waste. Across all scenarios, the electrode materials contribute the most to the reduction of GWP. These two components also have the highest value among the battery components, providing more incentive to focus recycling on these components.

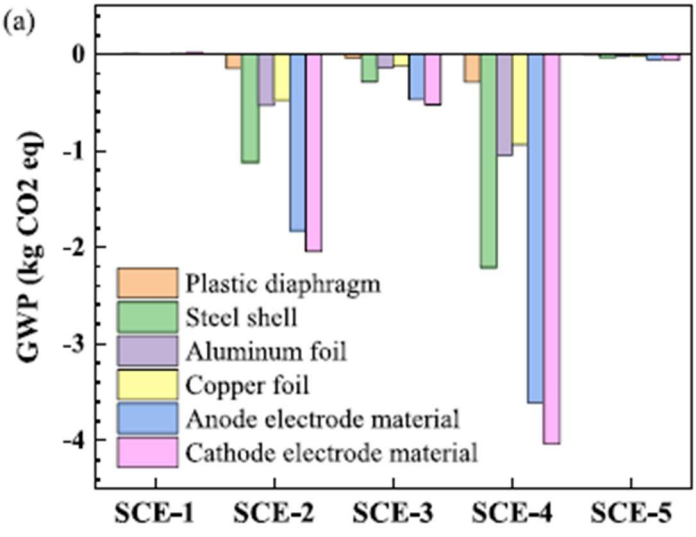

Figure 42. GWP associated with LiB components (Yang et al., 2024)

A similar study conducted by Kallitsis et al. (2022) compared the environmental impacts of the pyrometallurgical and hydrometallurgical routes of recycling lithium-ion batteries. Both processes were evaluated across 13 impact categories (see Appendix 11 for definition).

Table 9 and Table 10 outline the environmental impacts of the hydrometallurgical and pyrometallurgical recycling routes, respectively.

Table 9. Environmental impact of battery production, burden and benefit of hydrometallurgical battery recycling and their combined effect in the environmental footprint of an NMC333-Gr battery pack (Kallitsis et al., 2022).

Impact per capacity [kW h] Units		Production Impact	Hydrometallurgical case			
			Burden	Benefit	Total	Net [%]
GWP	kg CO_2-eq	168.8	12.7	-77.7	103.7	-39
FDP	kg oil-eq	59.8	3.96	-28.7	35.1	-41
SODP	kg CFC-11-eq	9.3×10^{-5}	7.2×10^{-6}	-5.8×10^{-5}	4.2×10^{-5}	-55
POFP	kg NOx-eq	0.508	0.04	-0.278	0.265	-48
FPMFP	kg $PM_{2.5}$-eq	0.906	0.035	-0.672	0.269	-70
TAP	kg SO_2-eq	2.61	0.076	-2.01	0.68	-74
FEP	kg P-eq	0.32	0.018	-0.23	0.11	-67
MEP	kg N-eq	0.019	3.21×10^{-3}	-0.013	0.009	-52
FETP	kg 1,4-DCB-eq	15.0	19.1	-10.0	24.1	60
METP	kg 1,4-DCB-eq	22.1	23.0	-15.2	39.9	35
TETP	kg 1,4-DCB-eq	7932	286	-6411.6	1806	-77
HTP	kg 1,4-DCB-eq	24.2	5.02	-18.9	12.2	-53
MDP	kg Cu-eq	6.09	0.299	-13.4	2.60	-84

Table 10. Environmental impact of battery production, burden and benefit of pyrometallurgical battery recycling and their combined effect in the environmental footprint of an NMC333-Gr battery pack (Kallitsis et al., 2022).

Impact per capacity [kW h] Units		Production Impact	Pyrometallurgical case			
			Burden	Benefit	Total	Net [%]
GWP	kg CO_2-eq	168.8	15.8	-74.9	109.8	-35
FDP	kg oil-eq	59.8	4.81	-27.8	36.7	-39
SODP	kg CFC-11-eq	9.3×10^{-5}	7.5×10^{-6}	-5.7×10^{-5}	4.32×10^{-5}	-54
POFP	kg Nox-eq	0.508	0.05	-0.270	0.283	-44
FPMFP	kg $PM_{2.5}$-eq	0.906	0.037	-0.671	0.271	-70
TAP	kg SO_2-eq	2.61	0.074	-2.00	0.69	-74
FEP	kg P-eq	0.32	0.018	-0.23	0.11	-66
MEP	kg N-eq	0.019	3.21×10^{-3}	-0.012	0.011	-45
FETP	kg 1,4-DCB-eq	15.0	19.1	-10.0	24.1	61
METP	kg 1,4-DCB-eq	22.1	22.9	-15.1	30.0	35
TETP	kg 1,4-DCB-eq	7932	279	-6398.8	1813	-77
HTP	kg 1,4-DCB-eq	24.2	5.07	-18.7	12.5	-52
MDP	kg Cu-eq	6.09	0.308	-12.4	3.66	-77

Across the impact categories, the hydrometallurgical route shows a slightly lower burden in the process due to the additional materials recovered (i.e., lithium), as well as a higher benefit, which is due to a less energy-intensive process. This is especially true for the energy

requirement of the pyrometallurgical process, which increases the GWP burden on the recycling process. In either recycling process, there is at least a 35% reduction across the 11 impact categories out of 13.

The remaining two categories, Freshwater Ecotoxicity Potential (FETP) and Marine Ecotoxicity Potential (METP), have an opposite effect. Over 96% of the burden of these two categories are attributed to the preparation of aluminum scraps. This is mostly the case for the environmental burdens of the toxicity and ecotoxicity categories, where the recovery chains of copper, aluminum and steel are the major contributors (Kallitsis et al., 2022). Meanwhile, the recovery of cathode active materials showed a significant impact on air quality, toxicity and resource depletion categories. This highlights the importance of establishing sustainable LiB recycling chains by focusing on the circularity aspect at the pack level of batteries.

The contribution of the impact from Al and Cu recovery calls for the question of unlocking the circularity of battery recycling from cell level to pack level. The recovery of metals, along with the batteries' active material, can lead to a more economical and sustainable battery recycling. In addition, it is suggested that battery recycling processes should be combined with sustainable production processes, renewable energy utilization and ensuring longevity of battery systems (technological development). This could lead to a significant impact on the cradle-to-grave footprint associated with LiB (Kallitsis et al., 2022).

Summary and Conclusions

The increased demand of lithium-ion batteries has driven the criticality of the raw materials such as lithium, nickel, manganese and cobalt. This poses risks in the supply security and economic importance in the European Union. While recycling methods are in place to recover battery components, there is a need to recover the lithium component as set by the European Commission with the increasing criticality of lithium. Methods of recycling LiB include pyrometallurgical, hydrometallurgical and direct recycling. This study focuses on integrating a lithium recovery step to the hydrometallurgical method of recycling.

In this study, lithium is recovered as lithium carbonate through precipitation. Precipitation is carried by reacting a solution containing lithium sulfate with sodium carbonate, or a novel method of CO_2 bubbling. Parameters such as reaction time, temperature and amount of precipitating agent were considered in both setups.

Optimization experiments show that the optimal reaction time, temperature and stoichiometry for the precipitation with Na_2CO_3 is 1 hour, 90°C, and 120%, respectively. This corresponds to a total lithium recovery and solid purity of 50.91% and 97.10%. Meanwhile, the optimal reaction time, temperature and gas flow rate for the precipitation with CO_2 is 3 hours, 90°C, and 200 mL/min of CO_2, respectively. This corresponds to 64.12% lithium recovery and 96.7% purity of the recovered solid. Further tests are needed to optimize the effect of stoichiometry in the precipitation with Na_2CO_3, as well as the effect of reaction time in the precipitation with CO_2 and more effective NaOH dosage.

From the characterization tests, it was found that sodium sulfate is the main impurity of the process, especially in the CO_2 precipitation because of the addition of NaOH. The temperature, time and precipitant dosage have an important effect on lithium recovery and purity. Temperature has a positive effect on both lithium recovery and purity. Time has a positive effect on recovery and negative effect on purity. Meanwhile, precipitant dosage has a positive effect on recovery and negative effect on purity.

SEM imaging shows that the recycled lithium carbonate has a slightly different morphology from the pristine lithium carbonate. Recycled Li_2CO_3 shows a higher crystal size. The difference in morphology does not affect lithiation experiment as both lithiation products show the same morphology. Electrochemical testing has indicated that recycled batteries are comparable to batteries made from pristine materials in terms of capacity and stability, with 93% of the battery capacity and 100% of the Coulombic efficiency obtained.

Economically, the lithium recovery step has a net gain on the hydrometallurgical recycling plant due to the high cost of lithium carbonate. Between the precipitation methods, the CO_2 absorption unit has more operating costs due to additional operations and reagents, but it has a margin for the optimization of NaOH dosage and reaction time and an important reduction in the environmental impact (CO_2 capture).

References

Asenbauer, J., Eisenmann, T., Kuenzel, M., Kazzazi, A., Chen, Z., & Bresser, D. (2020). The success story of graphite as a lithium-ion anode material-fundamentals, remaining challenges, and recent developments including silicon (oxide) composites. In *Sustainable Energy and Fuels* (Vol. 4, Issue 11, pp. 5387–5416). Royal Society of Chemistry. https://doi.org/10.1039/d0se00175a

Chen, L., Tang, X., Zhang, Y., Li, L., Zeng, Z., & Zhang, Y. (2011). Process for the recovery of cobalt oxalate from spent lithium-ion batteries. *Hydrometallurgy*, *108*(1–2), 80–86. https://doi.org/10.1016/j.hydromet.2011.02.010

Chen, X., Chen, Y., Zhou, T., Liu, D., Hu, H., & Fan, S. (2015). Hydrometallurgical recovery of metal values from sulfuric acid leaching liquor of spent lithium-ion batteries. *Waste Management*, *38*(1), 349–356. https://doi.org/10.1016/j.wasman.2014.12.023

Davis, K., & Demopoulos, G. P. (2023). Hydrometallurgical recycling technologies for NMC Li-ion battery cathodes: current industrial practice and new R&D trends. In *RSC Sustainability* (Vol. 1, Issue 8, pp. 1932–1951). Royal Society of Chemistry. https://doi.org/10.1039/d3su00142c

Di Persio, F., Perez de Lucía, A., Gramendola, F., Palma, J., Acosta, M., Ferret, R., Carlos Viera Gabriela Benveniste, J., Manuel Pérez, J., Casasola Fernández, R., Medina, C., Peixoto, T., Rodríguez-Chueca, J., & Pérez, J. (2022). Reciclado de baterías de iones de litio de vehículo eléctricos. *Iniciativa Tecnológica Prioritaria* , *01*(2022).

European Commission. (2020). *Critical Raw Materials Resilience: Charting a Path towards greater Security and Sustainability*. http://info.worldbank.org/governance/wgi/.

Gaines, L. (2023). Driving the Battery Cell Revolution. In *Chemistry World Webinar*.

Gaines, L., Richa, K., & Spangenberger, J. (2018). Key issues for Li-ion battery recycling. In *MRS Energy and Sustainability* (Vol. 5, Issue 1). Springer Nature. https://doi.org/10.1557/mre.2018.13

Garcia, E. M., Santos, J. S., Pereira, E. C., & Freitas, M. B. J. G. (2008). Electrodeposition of cobalt from spent Li-ion battery cathodes by the electrochemistry quartz crystal microbalance technique. *Journal of Power Sources*, *185*(1), 549–553. https://doi.org/10.1016/j.jpowsour.2008.07.011

Garole, D. J., Hossain, R., Garole, V. J., Sahajwalla, V., Nerkar, J., & Dubal, D. P. (2020). Recycle, Recover and Repurpose Strategy of Spent Li-ion Batteries and Catalysts: Current Status and Future Opportunities. In *ChemSusChem* (Vol. 13, Issue 12, pp. 3079–3100). Wiley-VCH Verlag. https://doi.org/10.1002/cssc.201903213

Gratz, E., Sa, Q., Apelian, D., & Wang, Y. (2014). A closed loop process for recycling spent lithium ion batteries. *Journal of Power Sources*, *262*, 255–262. https://doi.org/10.1016/j.jpowsour.2014.03.126

Grützke, M., Mönnighoff, X., Horsthemke, F., Kraft, V., Winter, M., & Nowak, S. (2015). Extraction of lithium-ion battery electrolytes with liquid and supercritical carbon dioxide and additional solvents. *RSC Advances*, *5*(54), 43209–43217. https://doi.org/10.1039/c5ra04451k

Han, B., Anwar Ul Haq, R., & Louhi-Kultanen, M. (2020). Lithium carbonate precipitation by homogeneous and heterogeneous reactive crystallization. *Hydrometallurgy*, *195*. https://doi.org/10.1016/j.hydromet.2020.105386

Harper, G., Sommerville, R., Kendrick, E., Driscoll, L., Slater, P., Stolkin, R., Walton, A., Christensen, P., Heidrich, O., Lambert, S., Abbott, A., Ryder, K., Gaines, L., & Anderson, P. (2019). Recycling lithium-ion batteries from electric vehicles. In *Nature* (Vol. 575, Issue 7781, pp. 75–86). Nature Publishing Group. https://doi.org/10.1038/s41586-019-1682-5

Jara, A. D., & Kim, J. Y. (2020). Chemical purification processes of the natural crystalline flake graphite for Li-ion Battery anodes. *Materials Today Communications*, *25*. https://doi.org/10.1016/j.mtcomm.2020.101437

Kallitsis, E., Korre, A., & Kelsall, G. H. (2022). Life cycle assessment of recycling options for automotive Li-ion battery packs. *Journal of Cleaner Production*, *371*. https://doi.org/10.1016/j.jclepro.2022.133636

Latini, D., Vaccari, M., Lagnoni, M., Orefice, M., Mathieux, F., Huisman, J., Tognotti, L., & Bertei, A. (2022). A comprehensive review and classification of unit operations with assessment of outputs quality in lithium-ion battery recycling. In *Journal of Power Sources* (Vol. 546). Elsevier B.V. https://doi.org/10.1016/j.jpowsour.2022.231979

Li, J., Liang, G., Zheng, W., Zhang, S., Davey, K., Pang, W. K., & Guo, Z. (2023). Addressing cation mixing in layered structured cathodes for lithium-ion batteries: A critical review. In *Nano Materials Science* (Vol. 5, Issue 4, pp. 404–420). KeAi Communications Co. https://doi.org/10.1016/j.nanoms.2022.09.001

Ma, X., Chen, M., Zheng, Z., Bullen, D., Wang, J., Harrison, C., Gratz, E., Lin, Y., Yang, Z., Zhang, Y., Wang, F., Robertson, D., Son, S. B., Bloom, I., Wen, J., Ge, M., Xiao, X., Lee, W. K., Tang, M., … Wang, Y. (2021). Recycled cathode materials enabled superior performance for lithium-ion batteries. *Joule*, *5*(11), 2955–2970. https://doi.org/10.1016/j.joule.2021.09.005

Or, T., Gourley, S. W. D., Kaliyappan, K., Yu, A., & Chen, Z. (2020). Recycling of mixed cathode lithium-ion batteries for electric vehicles: Current status and future outlook. In *Carbon Energy* (Vol. 2, Issue 1, pp. 6–43). Blackwell Publishing Inc. https://doi.org/10.1002/cey2.29

Sabisch, J. E. C., Anapolsky, A., Liu, G., & Minor, A. M. (2018). Evaluation of using pre-lithiated graphite from recycled Li-ion batteries for new LiB anodes. *Resources, Conservation and Recycling*, *129*, 129–134. https://doi.org/10.1016/j.resconrec.2017.10.029

Singh, P., Sunder, M., Campbell, E., & Palmer, L. (2020, February 1). A Case Study of Nickel Dendritic Growth on Printed-Circuit Boards. *2020 Pan Pacific Microelectronics Symposium, Pan Pacific 2020*. https://doi.org/10.23919/PanPacific48324.2020.9059398

Sloop, S., Crandon, L., Allen, M., Koetje, K., Reed, L., Gaines, L., Sirisaksoontorn, W., & Lerner, M. (2020). A direct recycling case study from a lithium-ion battery recall. *Sustainable Materials and Technologies*, *25*. https://doi.org/10.1016/j.susmat.2020.e00152

Thompson, D. L., Hartley, J. M., Lambert, S. M., Shiref, M., Harper, G. D. J., Kendrick, E., Anderson, P., Ryder, K. S., Gaines, L., & Abbott, A. P. (2020). The importance of design in lithium ion battery recycling-a critical review. In *Green Chemistry* (Vol. 22, Issue 22, pp. 7585–7603). Royal Society of Chemistry. https://doi.org/10.1039/d0gc02745f

Velázquez-Martínez, O., Valio, J., Santasalo-Aarnio, A., Reuter, M., & Serna-Guerrero, R. (2019). A critical review of lithium-ion battery recycling processes from a circular economy perspective. In *Batteries* (Vol. 5, Issue 4). MDPI. https://doi.org/10.3390/batteries5040068

Windisch-Kern, S., Gerold, E., Nigl, T., Jandric, A., Altendorfer, M., Rutrecht, B., Scherhaufer, S., Raupenstrauch, H., Pomberger, R., Antrekowitsch, H., & Part, F. (2022). Recycling chains for lithium-ion batteries: A critical examination of current challenges, opportunities and process dependencies. In *Waste Management* (Vol. 138, pp. 125–139). Elsevier Ltd. https://doi.org/10.1016/j.wasman.2021.11.038

Yang, H., Hu, X., Zhang, G., Dou, B., Cui, G., Yang, Q., & Yan, X. (2024). Life cycle assessment of secondary use and physical recycling of lithium-ion batteries retired from electric vehicles in China. *Waste Management*, *178*, 168–175. https://doi.org/10.1016/j.wasman.2024.02.034

Yi, C. P., & Majid, S. R. (2018). The Electrochemical Performance of Deposited Manganese Oxide-Based Film as Electrode Material for Electrochemical Capacitor Application. In *Semiconductors - Growth and Characterization*. InTech. https://doi.org/10.5772/intechopen.71957

Zhang, G., Du, Z., He, Y., Wang, H., Xie, W., & Zhang, T. (2019). A sustainable process for the recovery of anode and cathode materials derived from spent lithium-ion batteries. *Sustainability (Switzerland)*, *11*(8). https://doi.org/10.3390/su11082363

Zhao, C., Zhang, Y., Cao, H., Zheng, X., Van Gerven, T., Hu, Y., & Sun, Z. (2019). Lithium carbonate recovery from lithium-containing solution by ultrasound assisted precipitation. *Ultrasonics Sonochemistry*, *52*, 484–492. https://doi.org/10.1016/j.ultsonch.2018.12.025

Appendices

Appendix 1. Recoverable lithium carbonate using sodium carbonate

		Time (h)			
Temp (°C)	Na_2CO_3 loading (%)	0.25	0.5	1	2
50	110	-	-	-	10.26%
	120	-	-	-	21.97%
70	110	49.25%	50.78%	52.30%	63.31%
	120	53.78%	63.35%	65.60%	63.54%
90	110	60.09%	68.91%	71.20%	71.72%
	120	70.14%	67.04%	77.12%	77.97%
	200	-	80.33%	89.26%	88.72%

Appendix 2. Total lithium carbonate recovered using sodium carbonate

		Time (h)			
Temp (°C)	Na_2CO_3 loading (%)	0.25	0.5	1	2
50	110	-	-	-	5.46%
	120	-	-	-	11.70%
70	110	29.42%	30.33%	31.24%	37.82%
	120	32.13%	37.84%	39.19%	37.96%
90	110	39.67%	45.49%	47.00%	47.34%
	120	46.30%	48.61%	50.91%	51.47%
	200	-	53.03%	58.93%	58.57%

Appendix 3. Lithium carbonate purity with sodium carbonate precipitation

		Time (h)			
Temp (°C)	Na_2CO_3 loading (%)	0.25	0.5	1	2
50	110				90.10%
	120				92.18%
70	110		98.08%	96.76%	96.86%
	120		94.58%		94.12%
90	110	94.29%		98.36%	93.88%
	120		99.07%		99.26%
	200	-	95.86%	96.26%	96.29%

Appendix 4. Recoverable lithium carbonate using carbon dioxide

		Time (h)		
Temp (°C)	CO_2 flow (mL/min)	1	2	3
70	150	10.57%	41.53%	67.09%
	200	36.03%	50.57%	64.73%
90	100	0.00%	53.18%	68.24%
	150	63.24%	63.79%	78.50%
	200	38.04%	74.27%	97.12%

Appendix 5. Total lithium carbonate recovered using carbon dioxide

		Time (h)		
Temp (°C)	CO_2 flow (mL/min)	1	2	3
70	150	6.32%	24.81%	40.08%
	200	21.53%	30.21%	38.67%
90	100	0.00%	35.10%	45.05%
	150	41.75%	42.11%	51.82%
	200	25.12%	49.03%	64.12%

Appendix 6. Lithium carbonate purity with carbon dioxide precipitation

Purity		Time	
Temp	Stoich	2	3
70	150	-	-
	200	96.11%	94.38%
90	100	-	-
	150	-	-
	200	97.10%	95.44%

Appendix 7. Heat and Power Requirement of Na_2CO_3 Precipitation

Temp (°C)	Residence Time (hr)	E tot	E sens (kWh)	W (kWh)	η
70	0.25	291.107	290.1935	13.52	0.9969
70	0.5	292.021	290.1935	27.04	0.9937
70	1	293.849	290.1935	54.07	0.9876
70	2	297.505	290.1935	108.15	0.9754
70	3	301.16	290.1935	162.22	0.9636
90	0.25	417.277	415.7926	13.35	0.9964
90	0.5	418.761	415.7926	26.69	0.9929
90	1	421.729	415.7926	53.39	0.9859
90	2	427.666	415.7926	106.77	0.9722
90	3	433.602	415.7926	160.16	0.9589
90	1	421.729	415.7926	53.54	0.9859

Appendix 8. Heat and Power Requirement of CO_2 Precipitation

Temp (°C)	Residence Time (hr)	E sens (kWh)	W (kWh)	η	E tot
90	0.25	1247.3778	117.36	0.9976	1250.434637
90	0.5	1247.3778	234.72	0.9951	1253.491458
90	1	1247.3778	469.44	0.9903	1259.605101
90	2	1247.3778	938.87	0.9808	1271.832387
90	3	1247.3778	1408.31	0.9714	1284.059672
70	0.25	870.5806	118.87	0.9978	872.462105
70	0.5	870.5806	237.74	0.9957	874.343655
70	1	870.5806	475.49	0.9914	878.1067548
70	2	870.5806	950.97	0.9830	885.6329545
70	3	870.5806	1426.46	0.9747	893.1591541

Appendix 9. Power and labor cost among selected EU countries

	Spain	Italy	Portugal	Norway	Sweden	Denmark	EU average
Electricity cost (€/kWh)	0.147	0.1771	0.1381	0.0738	0.0896	0.1157	0.0743
Gas cost (€/kWh)	0.0547	0.0603	0.0571	0.0051	0.0998	0.0488	0.0631
Labor Cost (€/hr)	24.6	29.8	17	51.9	38.9	48.1	31.8

Appendix 10. Scale-up details

		Na_2CO_3 Precipitation	CO_2 Precipitation
Operating Conditions	Temp (°C)	90	90
	Residence Time (hr)	1	3
	Stoich or CO2 flow	1.2	200
	Volume/batch, m3	5.671001482	17.01300445
	Batches/y	8760	2920
Material Flow	Annual 5.0 M NaOH used (m3)	-	22224.97887
	Annual 12.5 M NaOH used (ton)	-	13512.78715
	Annual water used (ton)	-	13334.98732
	Na2CO3 used (tons)	1987.118919	-
	CO2 used (tons)	-	5058.63702
	tons Li2CO3/y	679.9516384	856.3014328
	Lithium Recoery	50.91%	64.12%
	Moisture removed, tons/y	113.7100519	143.2014791
Energy Flow	Reactor Heat (kWh)	421.7291161	1284.059672
	Annual Dryer Heat (kWh)	73917.46354	93088.42919
	Annual Filtration Power (kWh)	20398.54915	25689.04298
	Mixer Power (kWh)	-	608.2786108
	Imepller Power (kWh/batch)	53.54346346	1408.31
	Annual Heat Consumption (kWh)	3768264.52	3842542.673
	Annual Power Consumption (kWh)	489439.2891	5914131.606

Appendix 11. Life Cycle Impact Categories

Impact Category		Unit
GWP	Global Warming Potential	kg CO_2-eq
FDP	Fossil Depletion Potential	kg oil-eq
SODP	Stratospheric Ozone Depletion Potential	kg CFC-11-eq
POFP	Photochemical Oxidant Formation Potential, human health	kg NOx-eq
FPMFP	Fine Particulate Matter Formation Potential	kg $PM_{2.5}$-eq
TAP	Terrestrial Acidification Potential	kg SO_2-eq
FEP	Freshwater Eutrophication Potential	kg P-eq
MEP	Marine Eutrophication Potential	kg N-eq
FETP	Freshwater Ecotoxicity Potential	kg 1,4-DCB-eq
METP	Marine Ecotoxicity Potential	kg 1,4-DCB-eq
TETP	Terrestrial Ecotoxicity Potential	kg 1,4-DCB-eq
HTP	Human Toxicity Potential	kg 1,4-DCB-eq
MDP	Metal Depletion Potential	kg Cu-eq